RESEARCH MEMORANDUM

INVESTIGATION OF INTERFERENCE LIFT, DRAG, AND PITCHING MOMENT OF A SERIES OF TRIANGULAR-WING AND BODY COMBINATIONS AT A MACH NUMBER OF 1.94

By Donald E. Coletti

Langley Aeronautical Laboratory
Langley Field, Va.

NATIONAL ADVISORY COMMITTEE
FOR AERONAUTICS

WASHINGTON

December 21, 1955

NATIONAL ADVISORY COMMITTEE FOR AERONAUTICS

RESEARCH MEMORANDUM

INVESTIGATION OF INTERFERENCE LIFT, DRAG, AND PITCHING MOMENT OF A SERIES OF TRIANGULAR-WING AND BODY COMBINATIONS AT A MACH NUMBER OF 1.94

By Donald E. Coletti

SUMMARY

An investigation was made at a Mach number of 1.94 of a series of triangular-wing and body combinations to determine the interference lift, drag, and pitching moment.

The models consisted of a series of seven flat-plate triangular wings of varying scale in combination with bodies of fineness ratio 9.13 and 10.27. Four wings had semiapex angles of 30°, whereas the remaining three wings had semiapex angles of 45°.

The results of the investigation indicated that interference between the wing and body gave an increase in lift over that of a wing and a body alone but at the expense of more drag. This interference also gave reductions in positive pitching moments. The effect of Reynolds number variation on the lift, drag, and pitching moment of the wing in the presence of the body was generally small. In general, good predictions of the interference lifts and pitching moments on the body due to the wings and on the wings due to the body were obtained by the methods presented in NACA RM A51J04 and NACA RM A52B06. Increasing the Mach number from 1.62 (NACA RM L55B25) to 1.94 (present results) did not change the interference lift contribution, eliminated the negative interference pitching moment on the wing due to the body, and decreased the interference drag contribution. Fineness ratio produced little or no effect on the interference quantities with the exception of the drag on the body due to the wing.

INTRODUCTION

The problems of wing-body-tail interference on various aircraft configurations have received considerable attention both theoretically and

experimentally at subsonic, transonic, and supersonic speeds. A compilation of much of the past work relating to these problems can be found in reference 1. Since the publication of reference 1, additional work has been done, some of which is presented in reference 2. In this reference, an experimental investigation was made at a Mach number of 1.62 to determine the interference aerodynamic characteristics of a series of triangular-wing and body combinations.

The present report can be considered an extension of reference 2 to include interference data of the same series of triangular-wing and body combinations but at a Mach number of 1.94. Similar to reference 2, the results presented herein place emphasis upon lift and pitching-moment interference, with drag interference results included. Comparisons of the measured interference quantities are made with theory. The investigation involved a series of flat-plate triangular wings of varying size having beveled leading and trailing edges in combination with a body of revolution having a fineness ratio of 10.27. Some additional tests were also made involving two of the triangular wings and a body having a fineness ratio of 9.13. Reynolds numbers of the tests varied from 0.25×10^6 to 2.46×10^6 based on the wing mean aerodynamic chord.

Four of the wings had semiapex angles of 30° with an exposed aspect ratio of 2.3, whereas the remaining three wings had semiapex angles of 45° with an exposed aspect ratio of 4.

SYMBOLS

α	angle of attack of body
b	total wing span
c_r	wing root chord
$\bar{c}$	mean aerodynamic chord of exposed wing
C_L	lift coefficient, Lift/qS
C_D	drag coefficient, Drag/qS
C_m	pitching-moment coefficient about 50 percent mean aerodynamic chord, Moment/qS$\bar{c}$
C_X	longitudinal-force coefficient for exposed wing in presence of body, X/qS

$C_{L_\alpha} = \frac{dC_L}{d\alpha}$ at $C_L = 0$

$C_{m_\alpha} = \frac{dC_m}{d\alpha}$ at $C_L = 0$

$C_{D_{min}}$	minimum drag coefficient
C_{L_α}'	lift-curve slope based on maximum body frontal area
C_{m_α}'	pitching-moment-curve slope based on maximum body frontal area and maximum body diameter
$C_{D_{min}}'$	minimum drag coefficient based on maximum body frontal area
d	body diameter
D	maximum body diameter
i	angle of wing incidence
L	total body length
M	Mach number
n	fineness ratio, L/D
l_f	forebody length from nose to juncture of body and leading edge of wing root chord
ϵ	semiapex angle of wing leading edge
q	dynamic pressure, $\rho V^2/2$
ρ	stream density
R	Reynolds number, $\rho V\bar{c}/\mu$
S	exposed wing area
t	maximum wing thickness
V	stream velocity
X	longitudinal force, positive rearward

[redacted]

x	longitudinal coordinate from nose of body
μ	coefficient of viscosity
A.C.	aerodynamic-center position relative to 50 percent mean aerodynamic chord, positive forward

Configuration identification:

B	body alone
W	exposed wing alone
WB	wing and body in combination
W(B)	wing in presence of body

Derived measurements:

b(w)	interference on body due to wing, $WB - [W(B) + B]$
w(b)	interference on wing due to body, $W(B) - W$

APPARATUS AND TESTS

Tunnel

The Langley 9-inch supersonic tunnel is a closed-throat, single-return, continuous-operating tunnel in which the test section is approximately 9 inches square. Different test Mach numbers are achieved through the use of interchangeable nozzle blocks. Eleven fine-mesh turbulence-damping screens are installed in the settling chamber ahead of the supersonic nozzle. The pressure, temperature, and humidity can be controlled during the tunnel operation.

Models

The basic models consisted of a body having interchangeable noses to give fineness ratios of 9.13 and 10.27 and of a series of seven flat-plate triangular wings of varying plan-form scale ratios having beveled leading and trailing edges. Four of the wings had semiapex angles of 30° (exposed aspect ratio of 2.3), whereas the remaining three wings had semiapex angles of 45° (exposed aspect ratio of 4). Table I gives the body coordinates and wing-shape parameters. A sketch of a typical triangular wing mounted on the two bodies of different forebody lengths

is shown in figure 1, and a photograph of all the models including the seven wings tested in the presence of the body, the n = 10.27 body, the nose for the n = 9.13 body, and the two wings tested alone (sting-mounted) is shown in figure 2.

An illustration showing how wings in the presence of the body are interchanged is shown in figure 2 of reference 3. However, for some of the wings of this investigation (wings 1, 2, 3, 5, and 6 - see fig. 2), slots had to be cut in the forward and rear center of the wings to fit the body. These slots were cut so that a small gap (0.003 inch) existed between the wing and body, thereby insuring a free-floating wing. The gap effect on the aerodynamic forces is believed to be negligible and is discussed in reference 2.

Balances

A strain-gage balance mounted inside the body was used to obtain the lift, drag, and pitching moment of the wings in the presence of the body. The housing containing this internal balance was closed off at the model and sting bases to prevent any flow of air through the housing at these points. For a detailed description of the balance, see reference 3.

The lift, drag, and pitching moment of the seven triangular-wing and body combinations of the two bodies alone and of the two wings alone were obtained by an external balance system. The various configurations were sting-mounted to a system of self-balancing beam scales. A detailed description of the installation of the test models and the elimination of the tare forces may also be found in reference 3.

Tests

Tests were conducted at a Mach number of 1.94. Measurements were made of lift, drag, and pitching moment about the wing 50 percent mean aerodynamic chord for the wings alone, bodies alone, wings in the presence of the bodies, and the wing-body combinations. Reynolds numbers of the tests based on the wing mean aerodynamic chord varied from 0.25×10^6 to 2.46×10^6. (For a detailed list of Reynolds numbers for the various wings, see table II.) The angle of attack of each configuration was indicated on a scale, graduated in degrees, by means of a light beam reflected from a small mirror mounted flush on the rear of the body and on the sting in the case of the wing alone. The range of angle of attack was approximately $\pm 6^\circ$.

Throughout the tests, the dewpoint in the tunnel was maintained at a level where condensation effects would be negligible.

PRECISION OF DATA

The precision of the various quantities involved in the testing is listed in table II. This extensive table results from the change in the accuracies of the coefficients with wing configuration. It is understandable that, for a given uncertainty of a particular quantity, the accuracy of the coefficient derived from this quantity would be a function of the S and $\bar{c}$ values. At the lower Reynolds numbers, the accuracies of some of the measured quantities (see blanks in table II) were insufficient to obtain reliable interference quantities. This may be attributed to the low loads on the model and its components at the lower Reynolds numbers and to the accuracy of the external balance system at the time of these tests. The present tests along with the tests reported in reference 2 were some of the first to utilize the recently installed six-component external balance system; consequently, the improved accuracy now obtained with the system and resulting from modifications to the balance subsequent to the tests of this investigation was lacking. The estimated uncertainties in a given quantity obtained from the strain-gage balance (wing in the presence of the body) were combined by the method which is based on the theory of least squares outlined in reference 4. For the case where the precision varies with the lift, the accuracy was determined at the approximate end of linearity of the lift.

The accuracy of the stream Mach number represents a maximum variation about a mean Mach number throughout the test section.

PRESENTATION OF DATA

In figures 3 to 20, the aerodynamic characteristics of C_L, C_D, C_X, and C_m of the wings alone, bodies alone, wings and bodies in combination, and wings in the presence of the bodies are presented as a function of angle of attack. All the coefficients are based on the exposed wing area of the particular configuration. Since the Reynolds numbers vary both with the wings and with tunnel stagnation pressure, the Reynolds numbers are given in the figures.

DISCUSSION OF RESULTS

Wing Alone, General

Lift-curve slopes, pitching-moment-curve slopes, and minimum drag of the wings alone were obtained by testing one wing from each group of wings having semiapex angles of 30° and 45°. These two wings were

tested over a range of Reynolds number equivalent to that which would be obtained if wings 1 to 7 were tested. Wings 2 and 6 were selected since their scale factors were such that equivalent Reynolds numbers could easily be obtained within the limits of the tunnel operation. The Reynolds numbers were obtained by varying the tunnel stagnation pressure. It is realized that the thickness ratios of wings 2 and 6 (wing alone, table I) do not correspond to all of the thickness ratios of wings from 1 to 7 (see table I). Therefore, some of the minimum drags cannot be compared directly even for equivalent Reynolds numbers. Corrective measures were not made to the data with regard to the thickness-ratio effect; discussions concerning this will be presented in later sections. The lift, drag, and pitching-moment coefficients of wings 2 and 6 are presented in figures 19 and 20, respectively, as functions of angle of attack for various values of Reynolds numbers. Lift-curve slopes, pitching-moment-curve slopes, and minimum drags are shown in figure 21 for wings 2 and 6. The coefficients corresponding to the Reynolds numbers of wings 1 to 7 obtained from the faired and extrapolated curves of figure 21 are tabulated in table III.

Wing in the Presence of the Body,

Reynolds Number Effect

The effect of Reynolds number on the aerodynamic characteristics for the wings in the presence of the two bodies is shown in figure 22. It is seen that, for the configurations investigated, the lift generally increases with increasing Reynolds numbers for any one wing. This small increase in lift is probably due to a decrease in separation at the wing trailing edge and body juncture in going from a low to a high Reynolds number. It is further seen that as the Reynolds number is increased, the pitching moment remains constant or decreases slightly for a given wing. This could also indicate a decreasing region of separation with increasing Reynolds number, and in turn cause a slight rearward shift of the aerodynamic center. It is, of course, realized that this slight decrease of pitching moment may not be too significant since for some wings this decrease is of the order of the accuracy of the measurements.

Figure 22 shows that for any one wing the drag is essentially constant for increasing Reynolds number. It is further seen from figure 22, that the smaller wings generally have higher drag coefficients than the larger wings with the same apex angle. This is, at least in part, due to the increase in wave drag that results from increasing thickness ratio with decreasing wing size (see table I and fig. 2). A substantiation of this was made by using an approximation involving ratios of $(t/c)^2$ for the wings.

Within the limits of this investigation and with a consideration of the accuracies of table III, there is no effect on the aerodynamic characteristics due to varying the forebody length.

Basic Quantities for Interference Evaluation

General.- Figures 23 and 24 show, for configurations involving wings having $\epsilon = 30^\circ$ and $\epsilon = 45^\circ$, respectively, the variation of lift-curve slope, pitching-moment-curve slope, and minimum drag values with ratios of b/D for the wing and body in combination WB, wing in the presence of the body W(B), body alone B, and the wing alone W. In these same figures, comparisons are made between experiment and theory of some of the configurations and coefficients. The experimental quantities are taken directly from the curves in figures 3 to 21. The coefficients of the wings and bodies alone are based on the exposed wing area and are presented as functions of b/D for consistence purposes and for the convenience of comparison with the remaining configurations.

Wings.- The theoretical lifts for the wings alone were obtained from reference 5. Brown's theory was used for the subsonic-leading-edge wing ($\epsilon = 30^\circ$ shown in fig. 23) and Ackeret's result was used for the supersonic-leading-edge wing ($\epsilon = 45^\circ$ shown in fig. 24). The theoretical values, while somewhat higher than those obtained experimentally, are nevertheless, in good agreement with the experimental values, particularly for the $\epsilon = 45^\circ$ wings.

Since linear theory predicts the center of pressure at the centroid of the area or 50 percent mean aerodynamic chord, the theoretical pitching moment is zero for this investigation.

Body.- The theoretical lifts and pitching moments for the body alone were obtained from the theory presented in reference 6. As seen from the figures, the theory is in good agreement with the experimental pitching moments and only fair with the experimental lifts. Theoretical values of lift for the n = 9.13 body (not shown) were slightly larger than the theoretical values for the n = 10.27 body and were of the same trend as the experimental values. The theoretical pitching moments for the n = 9.13 body (not shown) were found to be in very good agreement with the experimental values.

As seen in figure 23, the experimental lifts for the n = 9.13 body are slightly larger than are those for the n = 10.27 body. With consideration of the accuracies involved, there is no difference in experimental pitching moments between the two bodies. The increase in drag for the n = 9.13 body over that for the n = 10.27 body is, of course, due to the fineness-ratio effect.

[redacted]

Wings in presence of body.- The methods for predicting the lifts and pitching moments of the wings in the presence of the bodies are found in references 7 and 8. The predicted lifts for the $\epsilon = 30^{\circ}$ configurations are slightly high, but have the same trend as the experimental values. The predicted lifts for the $\epsilon = 45^{\circ}$ configurations are in very good agreement with the experimental lifts. The agreement between the experimental and predicted values of pitching moment is good for all the configurations. No differences are predicted in the lifts between the n = 9.13 body and the n = 10.27 body. This result occurred also for the pitching moments.

The minimum drag coefficients for all the wings in the presence of the bodies, shown in figures 23 and 24, do not take into account the effects due to the different thickness ratios. If these effects were considered, it is probable that the trend of drags would parallel that for the wings alone in going from a low to a high b/D. It is obvious then that the interference drag on the wing due to the body would also be affected.

Wing and body in combination.- The comparisons between the experimental lifts and pitching moments for the wing-body combinations and the methods presented in references 7 and 8 are in better agreement than are similar comparisons for the wings in the presence of the bodies. As seen in figures 23 and 24, the differences between the experimental and the predicted lifts for the wings in the presence of the bodies are slightly larger than are those for the wing and body combinations. The calculated forces and moments for the wing-body combinations were obtained in the same manner as were those for the wings in the presence of the bodies, namely, a percentage of the forces on the wing alone.

The experimental lifts for the wing-body combinations involving the n = 9.13 body are slightly larger than are those involving the n = 10.27 body. No differences were found in pitching moments between the wing-body combinations involving the two different forebody lengths. The drags of the combinations with the n = 9.13 body are slightly larger than are those with the n = 10.27 body.

Interference Quantities

General.- The interference on the body due to the wing is obtained by subtracting the forces on the wing in the presence of the body and body alone from that of the wing-body combination; that is, $b(w) = WB - \left[W(B) + B\right]$. In like manner, the interference on the wing due to the body is the difference between the forces on the wing in the presence of the body and on the wing alone in free stream; that is, $w(b) = W(B) - W$.

[redacted]

A summation of the interference quantities for the body due to the wing $b(w)$ and the wing due to the body $w(b)$ is presented as a function of b/D in figure 25 and c_r/D in figure 26 for the series of the wing and body combinations. In figure 25(a) and 25(b) the values are based on the exposed wing area since the methods of references 7 and 8 for the predictions of the interference quantities base the coefficients on the area of the exposed wing. In figures 25(c), 25(d), 26(a), and 26(b) the values are based on the maximum body frontal area and maximum body diameter. If differences between the interference forces on the body due to the wing are to be explained for the various wing-body combinations, it is understandable that erroneous conclusions could be made concerning some of the quantities with the coefficients based on the exposed wing area. For this reason, discussions concerning the effects between the various wing-body combinations will be confined to coefficients based on maximum body frontal area and maximum body diameter for the case of the body due to the wing and on exposed wing area for the case of the wing due to the body.

Theoretical methods used to predict the interference quantities indicated no differences between configurations involving the n = 9.13 body and the n = 10.27 body.

Lift on body due to wing.- A comparison of the experimental lift on the body due to the wing $b(w)$ with the theoretical method is shown in figure 25(a). In general, the agreement is good with the exception of the configuration involving wing 1 with a b/D value of 5.60. For this configuration the experimental lift is high. It is believed that this may be due to some interference phenomenon associated with the leading edges of wings 1, 2, 3, and 4 ($\epsilon = 30^\circ$) approaching a sonic condition. As seen from figure 25(a), the lift decreases with increasing b/D or exposed wing area; however, when the values are based on a common area (see figs. 25(c) and 26(a)), the interference lift increases with increasing wing size as would be expected. From figure 27, the interference lift on the body due to the wing is seen to be predominately that which carries over from the wing to the body between the Mach helices emanating from the leading- and trailing-edge root-chord junction. Figure 27 also indicates that with decreasing wing scale, the area upon which this interference lift acts decreases, resulting in less interference lift. From figure 26(a), the lift on the body due to the wing for any given c_r/D is less for configurations with wings having $\epsilon = 30^\circ$ than for those having $\epsilon = 45^\circ$. This is apparently due to the fact that the higher lift for the supersonic-leading-edge wing (as compared with that for the subsonic-leading-edge wing) carries over onto the body.

In addition to this positive carryover lift, an induced negative lift, created by the vortex action of the wing, acts on the afterbody. Since there were no definite results in the present investigation

pointing to this induced negative lift, it is probable that this lift represents a small percentage of the total interference. This was also found to be the condition that existed for the triangular wings in reference 2 and the rectangular wings in reference 3.

There appears to be little or no effect of forebody length on the interference lift of the body due to the wing as shown in figure 25(c).

Pitching moment for body due to wing.- Figure 25(a) shows that the agreement between the experimental and theoretical pitching moment for the body due to the wing is good at the high values of b/D but poor at the low values of b/D. Some of this poor agreement at the low values of b/D may be due to the low accuracy of the experimental measurements for the smaller wings. (See, for example, wing 4 in table II.)

With reference to the sketches in figure 27, the wing-root lift carryover onto the body acts behind the center of gravity so that a negative pitching moment is obtained. This is shown experimentally in figures 25 and 26.

With consideration of the accuracies, there appears to be no difference in experimental interference pitching moments on the body due to the wing for the different forebody lengths.

Aerodynamic center of body due to wing.- As seen in figure 25(a), the theoretical aerodynamic centers are in good agreement with the experimental results at high values of b/D and in fair agreement at low values of b/D. The variation of the aerodynamic centers with b/D shows that, for configurations having $\epsilon = 45^\circ$ wings, the interference lift center is farther rearward along the body than for the $\epsilon = 30^\circ$ configurations. If the aerodynamic centers were shown as functions of c_r/D values, the lift centers between the $\epsilon = 30^\circ$ and $\epsilon = 45^\circ$ configurations would be coincident.

The interference aerodynamic-center locations are about the same for configurations having different forebody lengths as seen in figure 25(a).

Drag on body due to wing.- When the coefficients are based on the exposed wing area as in figure 25(a), the interference drag on the body due to the wing $b(w)$ for the $\epsilon = 30^\circ$, $n = 10.27$ configurations decreases with increasing b/D. The $\epsilon = 45^\circ$ configurations follow the same trend with the exception of $b/D = 3.62$; the reason for the lower interference drag of this configuration is not known.

The reason for the lower $b(w)$ drag of the $n = 9.13$ configurations becomes more apparent when the equation for $b(w)$ is considered; that is, $b(w) = WB - \left[W(B) + B\right]$. For the lower fineness-ratio configurations,

the body-alone drag is higher, whereas the W(B) and WB drags remain essentially the same for the two configurations (table III), the net result being lower b(w) drag for the n = 9.13 configurations.

When the coefficients are based on the maximum body frontal area (figs. 25(c) and 26(a)) there is, in general, a slightly increasing b(w) drag with increasing b/D or c_r/D.

Lift on wing due to body.- Figure 25(b) shows that good agreement is obtained between the experimental lift on the wing due to the body w(b) and theory. With the coefficients based on the exposed wing area (fig. 25(b)), it is seen that higher lift coefficients are obtained on the smaller wings. In all probability this is due to the fact that more of the area of the smaller wings is in the stronger upwash field of the body compared with that for the larger wings. It is further seen that, for any given b/D, the interference lift coefficient is greater for the $\epsilon = 45^\circ$ configuration than for the $\epsilon = 30^\circ$ case. Of course, when the coefficients are based on the maximum body frontal area (figs. 25(d) and 26(b)), more positive lift coefficients are obtained from the larger wings.

The effect of changing forebody length had no effect on the interference lift on the wing due to the body.

Pitching moment of wing due to body.- With consideration of the accuracy the interference pitching moment of the wing due to the body, for all practical purposes, is negligible for configurations involving wings 3, 4, and 7 as shown by figures 25(b), 25(d), and 26(b). For configurations involving wings 1, 2, 5, and 6 a small positive moment is obtained.

Aerodynamic center of wing due to body.- The interference aerodynamic centers shown in figure 25(b) generally follow the same trends as the interference pitching moments. The location of the interference aerodynamic centers may be explained by the fact that for wings 1, 2, 5, and 6 the interference lift center is slightly forward of the centroid of the wing areas (resulting in a positive pitching moment), whereas for wings 3, 4, and 7 the interference lift center is very nearly coincident with the centroid of the wing areas or the 50 percent mean aerodynamic chord.

Drag on wing due to body.- The interference drags on the wings due to the body are shown in figures 25(b), 25(d), and 26(b). However, as was mentioned previously, the effect of wing thickness ratio (which was not taken into account in the analysis) would alter the variation of these drags. From estimations made to account for this thickness-ratio effect, the interference drags of figure 25(b) would be changed to give a more positive slope in going from low to high values of b/D. In any

case, most of the interference drag is apparently due to skin-friction effects.

Contributions of the Basic and Interference Quantities

In order to assess the relative effects of each quantity on the complete configuration, each of the basic and interference quantities of lift, pitching moment, and drag is shown in figure 28 as a function of the total lift, pitching moment, and drag of the complete configuration. Figure 28(a) presents the fractional breakdown of the various elements for the configurations involving the wings of $\epsilon = 30^\circ$ and bodies of $n = 10.27$ and $n = 9.13$; whereas figure 28(b) presents the configurations involving the wings of $\epsilon = 45^\circ$ and the $n = 10.27$ body. It is seen from this figure that the interference lift on the $w(b)$ and $b(w)$ is very beneficial for the configurations involving wings of $\epsilon = 30^\circ$ or 45°. Between a 17-percent and 36-percent increase in lift can be realized, because of interference, over that which could be obtained by simply adding the lifts of the wing alone and the body alone.

The pitching-moment contribution of the various lift quantities for all the wing-body combinations illustrates clearly that the lift on the $b(w)$ acts behind the centroid of the wing areas, thus giving a negative pitching moment. Between a 2-percent and a 34-percent reduction in positive pitching moment is realized because of interference over that which could be obtained by summing the pitching moments of the wing alone and of the body alone. The wing alone, wing in the presence of the body, and the interference on the wing due to the body contribute a positive pitching moment, showing that the lift center is ahead of the centroid of the wing area. The body moment contribution is by far the largest positive moment since its aerodynamic center is in the region of the nose of the body.

The fractional breakdown of the various drag quantities is somewhat as would be expected. That is, the low b/D wings alone contribute a smaller percentage of drag to the total than do the large b/D wings alone; whereas, the drag contribution of the body is the reverse. The drags for the $w(b)$ are presented as obtained from the tests with no corrections due to thickness ratio. The interference drags on the wing due to the body are seen to be small percentages of the total wing-body drags, whereas, the interference drags on the body due to the wings were a large percentage of the total with the exception of the configurations involving the $n = 9.13$ body.

A comparison of the interference quantities may be made at two different Mach numbers from the results of the present investigation ($M = 1.94$) and reference 2 ($M = 1.62$). In general, the beneficial contribution of interference lift to the total lift of any of the investigated

configurations is very nearly the same at the two Mach numbers. Positive interference pitching moments only were obtained on the wing due to the body at a Mach number of 1.94; whereas both positive and negative pitching moments were obtained at a Mach number of 1.62. The drag interference contribution is slightly less at $M = 1.94$ as compared with that at $M = 1.62$ for all the configurations investigated.

CONCLUSIONS

An investigation was made of the interference effects on a series of seven flat-plate triangular wings of varying scale in combination with bodies having two different forebody lengths. Four of the wings had semiapex angles of 30° while the remaining three had semiapex angles of 45°. Basic measurements of lift, drag, and pitching moment were obtained for the wing-body combinations, wing in the presence of the body, wing alone, and bodies alone at a Mach number of 1.94. Interference lifts, drags, and pitching moments were obtained from the basic measurements. The results indicate that:

1. Interference gave between a 17-percent and 36-percent increase in lift over that which would be obtained by summing the lifts of the wing alone and of the body alone. This was accompanied by an increase in drag due to skin friction.

2. The method presented in NACA RM A51J04 gave good predictions of the interference lifts on the body due to the wing and on the wing due to the body. The experimental lifts for the wing-body combinations and for the wings in the presence of the bodies were generally in good agreement with the above method.

3. Interference gave between a 2-percent and 34-percent reduction in positive pitching moment from that which would be obtained by summing the pitching moments of the wing alone and of the body alone.

4. The predictions of the interference pitching moments on the body due to the wings using the method in NACA RM A52B06 was in good agreement at the higher ratios of wing span to body diameter b/D and poor at the low b/D ratios. The experimental pitching moments for the wings in the presence of the body and the wing-body combinations were generally in good agreement with the above method.

5. Within the limits of this investigation, the effect of varying Reynolds number upon the lifts, drags, and pitching moments for the wings in the presence of the body was generally small.

6. The interference drags on the body due to the wings were a large percentage of the total wing-body drags, whereas the interference drags on the wings due to the body were relatively small percentages of the total drags. These interference drags were probably due to changes in skin-friction drags.

7. Within the limits of the investigation, changing the forebody length so that the fineness ratio, n, of the body changed from 9.13 to 10.27 had little or no effect on the interference quantities with the exception of the drag on the body due to the wing. This drag interference for the configuration involving the n = 9.13 body was considerably smaller than that for the configuration involving the n = 10.27 body.

8. Within the limits of this investigation and that presented in NACA RM L55B25, increasing the Mach number from 1.62 to 1.94 did not change the interference lift contribution, eliminated the negative interference pitching moment on the wing due to the body, and decreased the interference drag contribution.

Langley Aeronautical Laboratory,
National Advisory Committee for Aeronautics,
Langley Field, Va., September 14, 1955.

REFERENCES

1. Nielsen, Jack N., Kaattari, George E., and Anastasio, Robert F.: A Method for Calculating the Lift and Center of Pressure of Wing-Body-Tail Combinations at Subsonic, Transonic, and Supersonic Speeds. NACA RM A53G08, 1953.

2. Coletti, Donald E.: Investigation of Interference Lift, Drag, and Pitching Moment of a Series of Triangular Wing and Body Combinations at a Mach Number of 1.62. NACA RM L55B25, 1955.

3. Coletti, Donald E.: Investigation of Interference Lift, Drag, and Pitching Moment of a Series of Rectangular Wing and Body Combinations at Mach Numbers of 1.62, 1.93, and 2.41. NACA RM L52E26, 1952.

4. Michels, Walter C.: Advanced Electrical Measurements. Second ed., D. Van Nostrand Co., Inc., 1941.

5. Brown, Clinton E.: Theoretical Lift and Drag of Thin Triangular Wings at Supersonic Speeds. NACA Rep. 839, 1946. (Supersedes NACA TN 1183.)

6. Allen, H. Julian, and Perkins, Edward W.: Characteristics of Flow Over Inclined Bodies of Revolution. NACA RM A50L07, 1951.

7. Nielsen, Jack N., and Kaattari, George E.: Method for Estimating Lift Interference of Wing-Body Combinations at Supersonic Speeds. NACA RM A51J04, 1951.

8. Kaattari, George E., Nielsen, Jack N., and Pitts, William C.: Method for Estimating Pitching-Moment Interference of Wing-Body Combinations at Supersonic Speed. NACA RM A52B06, 1952.

TABLE I

BODY COORDINATES AND WING-SHAPE PARAMETERS

(SEE FIG. 1)

Body			Type	Flat-plate triangular wings												
x, in.	Diameter, in.			Designation	ϵ, deg	b/D	c_r/D	S, sq in.	c_r, in.	b, in.	$\bar{c}$, in.	i, deg	t, in.	t/$\bar{c}$	l_f, in. n = 10.27	l_f, in. n = 9.13
	n = 10.27	n = 9.13														
0	0.002	---		1	30	5.60	4.148	7.131	3.634	4.914	2.423	0.24	0.049	0.0202	2.850	-----
.500	.154	---														
1.000	.296	0		2	30	4.58	3.190	4.311	2.795	4.022	1.863	.01	.040	.0215	3.457	-----
1.500	.430	.262														
2.000	.552	.462		3	30	3.62	2.257	2.274	1.977	3.179	1.318	-.12	.031	.0235	4.273	3.273
2.500	.660	.620	Wing in													
3.000	.746	.728	presence	4	30	2.63	1.424	.900	1.248	2.312	.832	-.53	.020	.0240	4.685	3.685
3.500	.820	.814	of body													
3.750	.846	.846		5	45	7.41	3.213	7.947	2.815	6.497	1.876	-.01	.051	.0272	3.691	-----
4.000	.860	↑														
4.625	.872			6	45	5.69	2.338	4.209	2.048	4.991	1.365	-.06	.042	.0308	4.203	-----
5.000	.876															
5.500	.874			7	45	3.62	1.325	1.340	1.161	3.177	.774	-.15	.027	.0349	4.779	-----
6.000	.872	same as														
6.500	.866	n = 10.27														
7.250	.794															
8.000	.692			2	30	----	-----	4.281	2.789	3.070	1.859	----	.041	.0221	-----	-----
8.375	.628		Wing													
9.000	.500	↓	alone	6	45	----	-----	4.142	2.043	4.055	1.362	----	.042	.0308	-----	-----

TABLE II

SUMMARY OF TOTAL UNCERTAINTIES

Wing configuration	Body, n	R	Accuracy at $C_L = 0$ for WB, B, W			Accuracy at $C_L = 0$ for W(B)			Accuracy at approximate end of linearity for W(B)		Inaccuracy of slopes for WB, B, W		Inaccuracy of slopes for W(B)		Inaccuracies for b(w)			Inaccuracies for w(b)		
			C_L	C_m	C_D	C_L	C_m	C_D	C_L	C_m	C_{L_α}	C_{m_α}	C_{L_α}	C_{m_α}	C_{L_α}	C_{m_α}	$C_{D_{min}}$	C_{L_α}	C_{m_α}	$C_{D_{min}}$
1	10.27	0.82×10^6				±0.0005	±0.0002	±0.0002	±0.0007	±0.0005			±0.0004	±0.0002						
		2.46	±0.0001	±0.0004	±0.0001	±.0001	±.0001	±.0001	±.0002	±.0001	±0.0001	±0.0002	±.0001	±.0001	±0.0002	±0.0003	±0.0002	±0.0001	±0.0002	±0.0001
2	10.27	.63				±.0008	±.0004	±.0005	±.0011	±.0006			±.0006	±.0003						
		1.89	±.0002	±.0008	±.0001	±.0002	±.0001	±.0001	±.0004	±.0002	±.0001	±.0004	±.0002	±.0001	±.0002	±.0006	±.0002	±.0002	±.0004	±.0001
3	10.27	.45				±.0016	±.0010	±.0005	±.0023	±.0016			±.0012	±.0008						
		1.00				±.0006	±.0004	±.0002	±.0009	±.0007			±.0005	±.0004						
		1.33	±.0004	±.0022	±.0002	±.0005	±.0005	±.0002	±.0007	±.0005	±.0002	±.0011	±.0006	±.0005	±.0007	±.0016	±.0005	±.0006	±.0011	±.0005
3	9.15	.45				±.0016	±.0011	±.0006	±.0023	±.0016			±.0018	±.0008						
		1.32	±.0004	±.0022	±.0002	±.0005	±.0005	±.0002	±.0007	±.0005	±.0002	±.0011	±.0004	±.0005	±.0005	±.0016	±.0005	±.0004	±.0011	±.0005
4	10.27	.26				±.0041	±.0044	±.0018	±.0060	±.0066			±.0020	±.0033						
		.64				±.0016	±.0017	±.0006	±.0024	±.0026			±.0012	±.0012						
		.84	±.0009	±.0090	±.0006	±.0012	±.0013	±.0004	±.0017	±.0019	±.0005	±.0045	±.0009	±.0010	±.0010	±.0064	±.0009	±.0010	±.0046	±.0007
4	9.15	.27				±.0041	±.0044	±.0018	±.0060	±.0066			±.0050	±.0025						
		.85	±.0009	±.0091	±.0006	±.0012	±.0013	±.0004	±.0017	±.0019	±.0005	±.0046	±.0009	±.0010	±.0010	±.0066	±.0009	±.0010	±.0047	±.0007
5	10.27	.64				±.0004	±.0009	±.0001	±.0006	±.0005			±.0005	±.0002						
		1.90	±.0001	±.0005	±.0001	±.0001	±.0001	±.0001	±.0002	±.0001	±.0001	±.0003	±.0001	±.0001	±.0002	±.0004	±.0001	±.0001	±.0005	±.0001
6	10.27	.45				±.0008	±.0005	±.0005	±.0012	±.0008			±.0006	±.0004						
		1.40	±.0002	±.0012	±.0001	±.0005	±.0002	±.0001	±.0004	±.0002	±.0001	±.0006	±.0002	±.0001	±.0002	±.0008	±.0002	±.0002	±.0006	±.0001
7	10.27	.85				±.0026	±.0050	±.0009	±.0058	±.0045			±.0019	±.0025						
		.78	±.0006	±.0057	±.0004	±.0008	±.0029	±.0005	±.0018	±.0014	±.0005	±.0033	±.0006	±.0007	±.0007	±.0047	±.0006	±.0007	±.0034	±.0005

Configuration	Initial angle of attack	Relative angle of attack	Incidence angle of wings	Mach number	Reynolds number per inch	Stream pressure
All	±0.05°	±0.01°	±0.05°	±0.01	±12,000	±1.5 percent

TABLE III

SUMMARY OF LIFT-CURVE AND PITCHING-MOMENT-CURVE SLOPES,

AND MINIMUM DRAG VALUES AT ZERO LIFT FROM FIGURES 3 TO 21

Wing	Body, n	R	Wing-body combination, WB			Wing in presence of body, W(B)			[a]Wing, W			Body, B		
			C_{L_α}	C_{m_α}	$C_{D_{min}}$	C_{L_α}	C_{m_α}	$C_{D_{min}}$	C_{L_α}	C_{m_α}	$C_{D_{min}}$	C_{L_α}	C_{m_α}	$C_{D_{min}}$
1	10.27	0.82×10^6				0.0375	0.0013	0.0073						
		2.46	0.0553	0.0055	0.0215	.0414	.0015	.0084	0.0367	0.0008	0.0078	0.0022	0.0049	0.0069
2	10.27	.63				.0379	.0019	.0076						
		1.89	.0566	.0086	.0275	.0417	.0017	.0083	.0366	.0008	.0075	.0034	.0107	.0114
3	10.27	.45				.0428	.0024	.0077						
		1.00				.0438	.0019	.0079						
		1.33	.0644	.0254	.0402	.0436	.0019	.0080	.0365	.0010	.0056	.0069	.0304	.0217
3	9.13	.43				.0425	.0021	.0078						
		1.32	.0655	.0240	.0416	.0441	.0021	.0080	.0365	.0010	.0056	.0074	.0306	.0305
4	10.27	.26				.0465	.0015	.0086						
		.64				.0467	.0018	.0089						
		.84	.0825	.1024	.0906	.0467	.0018	.0097	.0357	.0011	.0052	.0172	.1210	.0548
4	9.13	.27				.0465	.0024	.0093						
		.85	.0877	.1005	.0889	.0480	.0016	.0093	.0357	.0011	.0052	.0186	.1215	.0771
5	10.27	.64				.0413	.0027	.0107						
		1.90	.0514	.0065	.0204	.0425	.0023	.0107	.0404	.0015	.0110	.0020	.0061	.0062
6	10.27	.45				.0430	.0033	.0115						
		1.40	.0585	.0138	.0290	.0459	.0027	.0113	.0404	.0016	.0108	.0039	.0160	.0117
7	10.27	.25				.0474	.0032	.0145						
		.78	.0733	.0784	.0530	.0482	.0032	.0126	.0398	.0020	.0089	.0122	.0887	.0367

[a]Data obtained at equivalent Reynolds numbers.

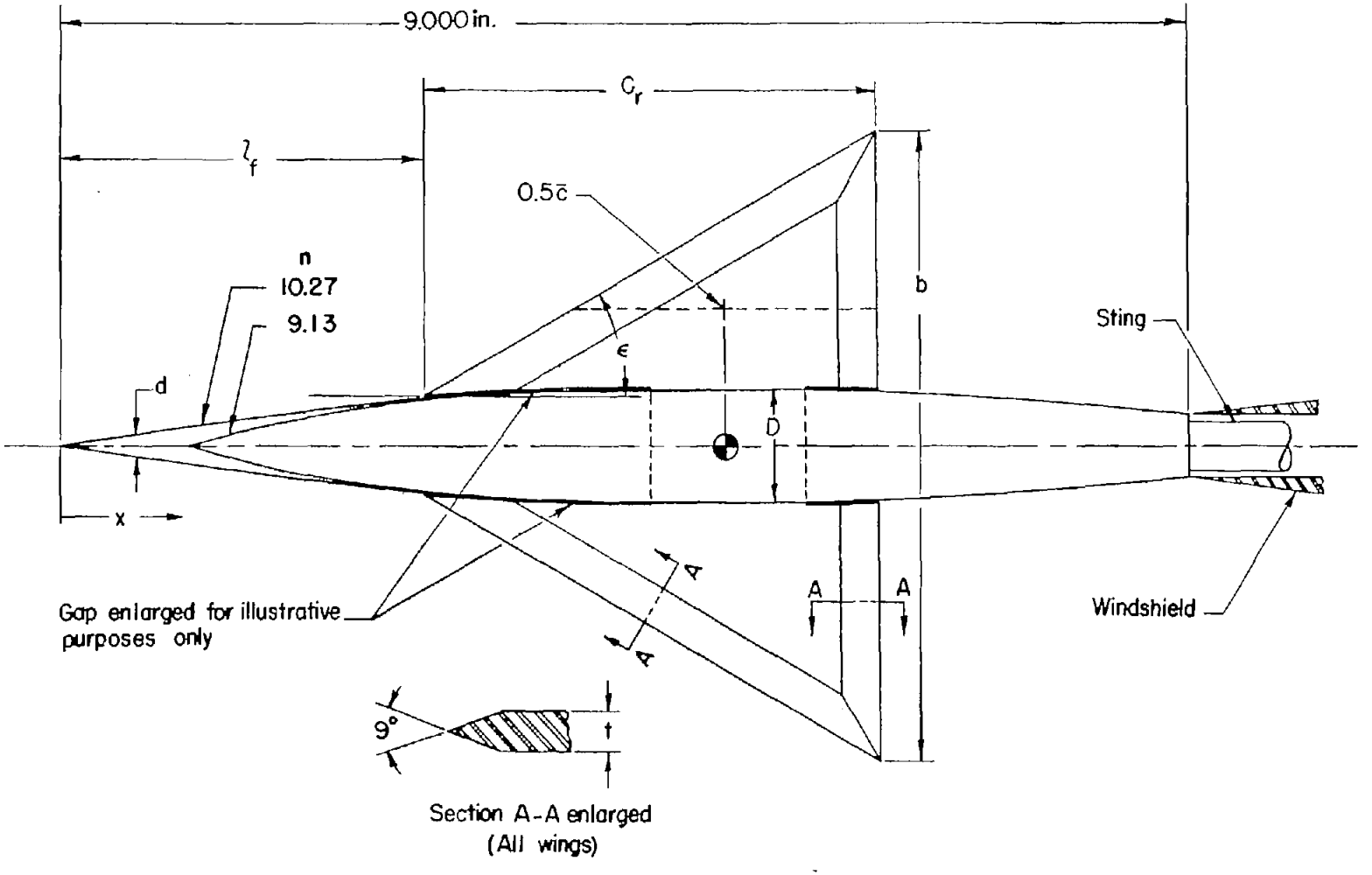

Figure 1.- Sketch of a triangular wing mounted on either an n = 10.27 body or an n = 9.13 body. Body coordinates and wing-shape parameters are listed in table I.

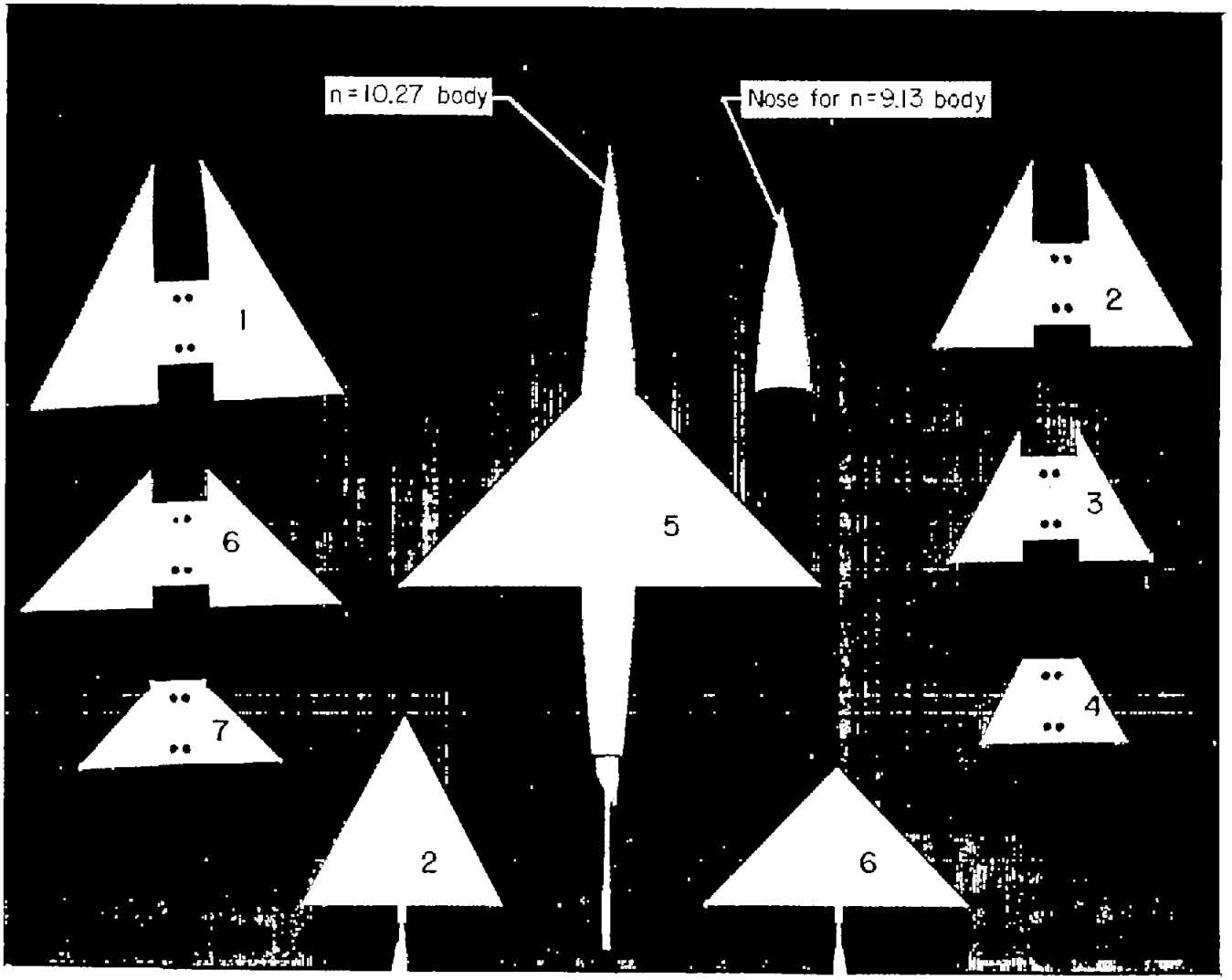

Figure 2.- Photograph of models tested.

L-89389

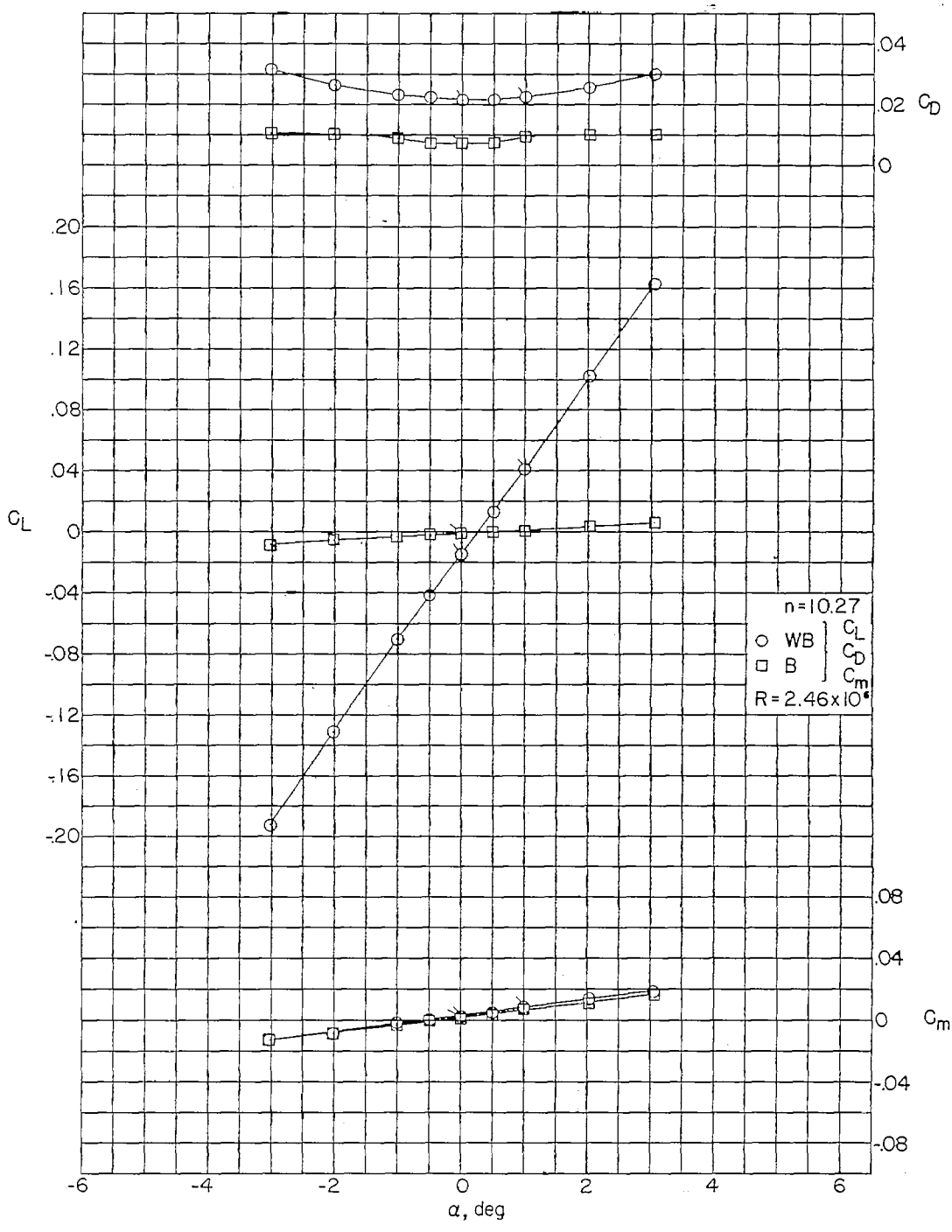

Figure 3.- Aerodynamic characteristics of the wing and body combination for triangular wing 1 ($\epsilon = 30^\circ$) and the n = 10.27 body alone. (Body-alone results are based on exposed area of triangular wing 1.) Flagged symbols denote check values.

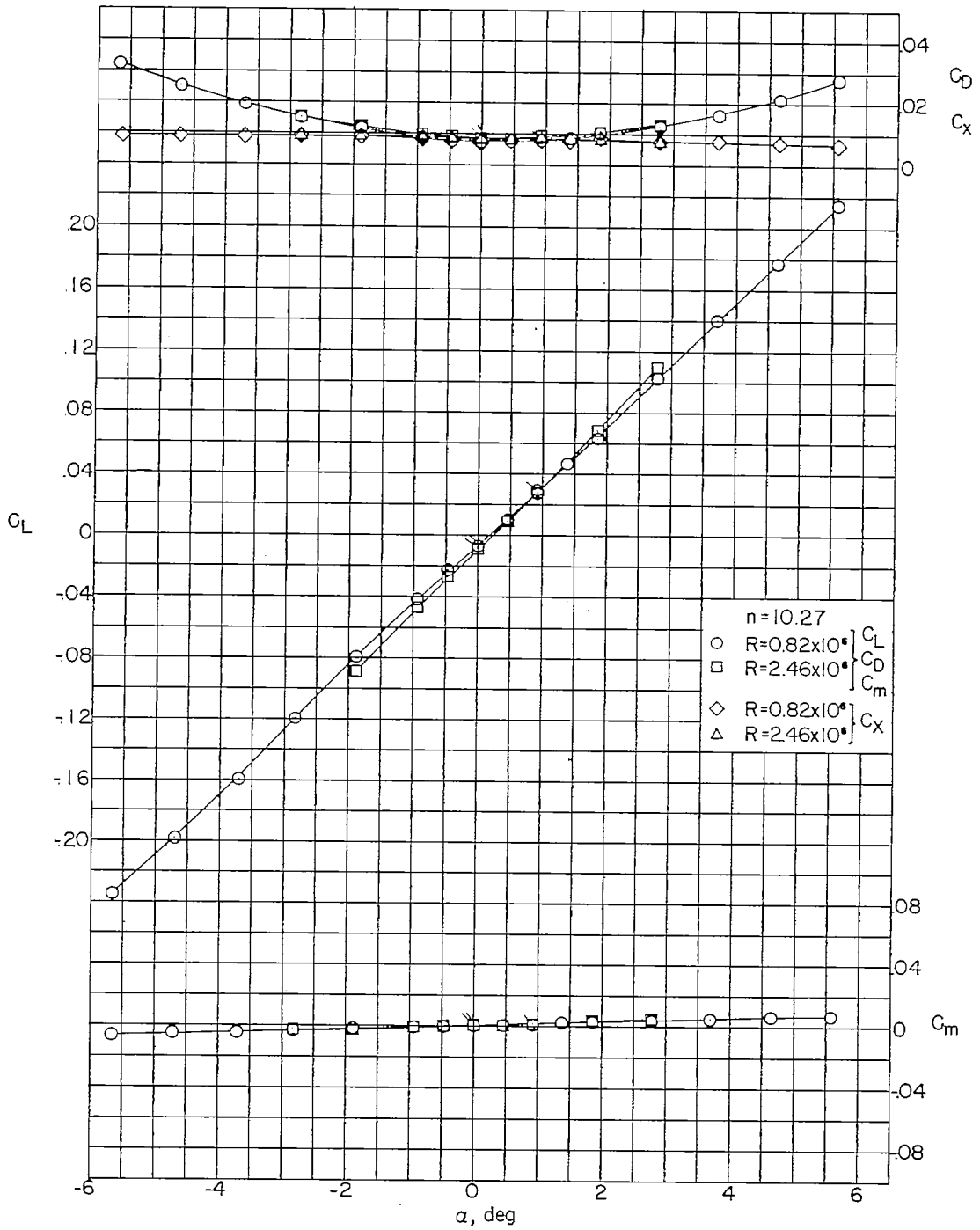

Figure 4.- Aerodynamic characteristics of the wing in the presence of the n = 10.27 body for triangular wing 1 ($\epsilon = 30^\circ$). Flagged symbols denote check values.

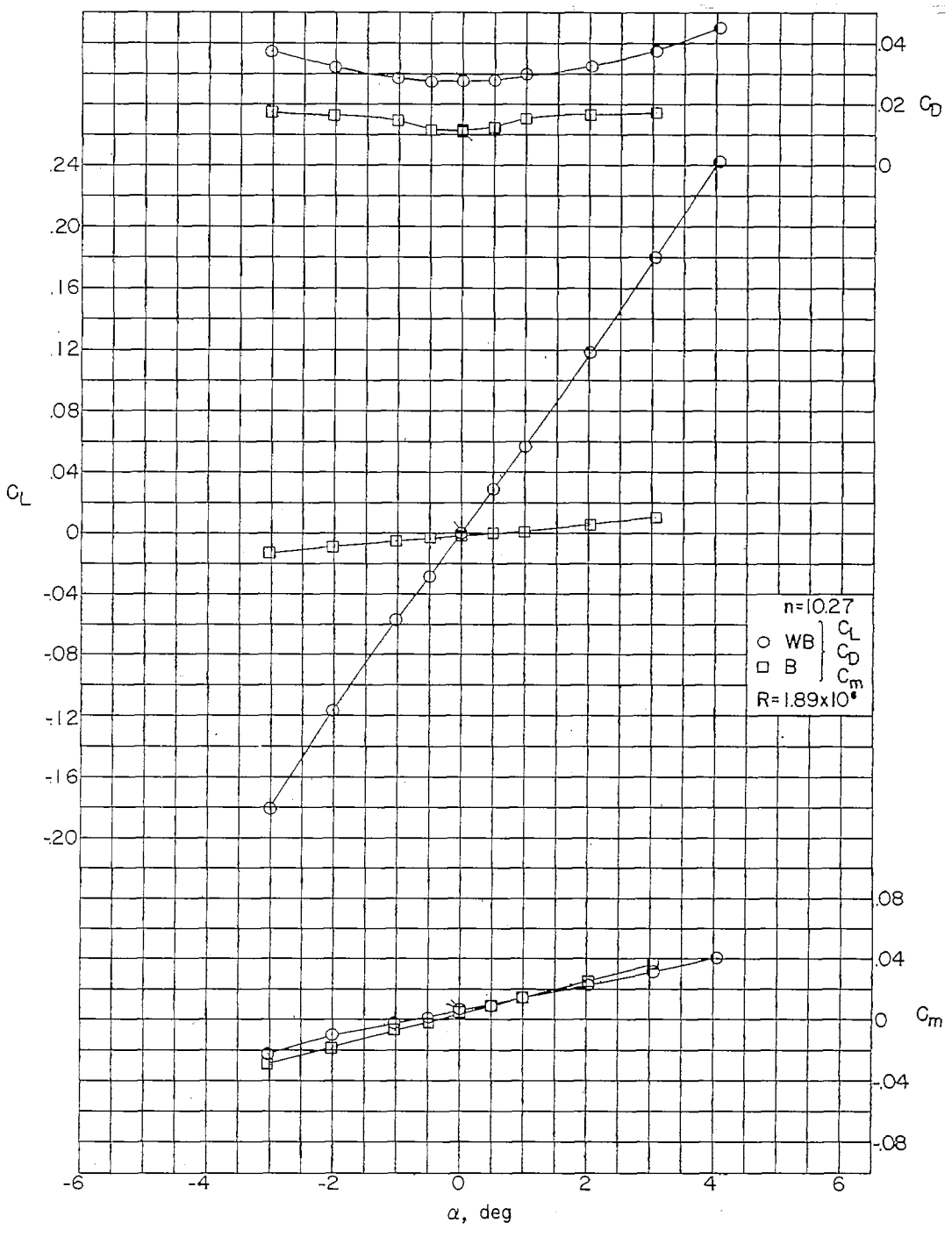

Figure 5.- Aerodynamic characteristics of the wing and body combination for triangular wing 2 ($\epsilon = 30^\circ$) and the n = 10.27 body alone. (Body-alone results are based on exposed area of triangular wing 2.) Flagged symbols denote check values.

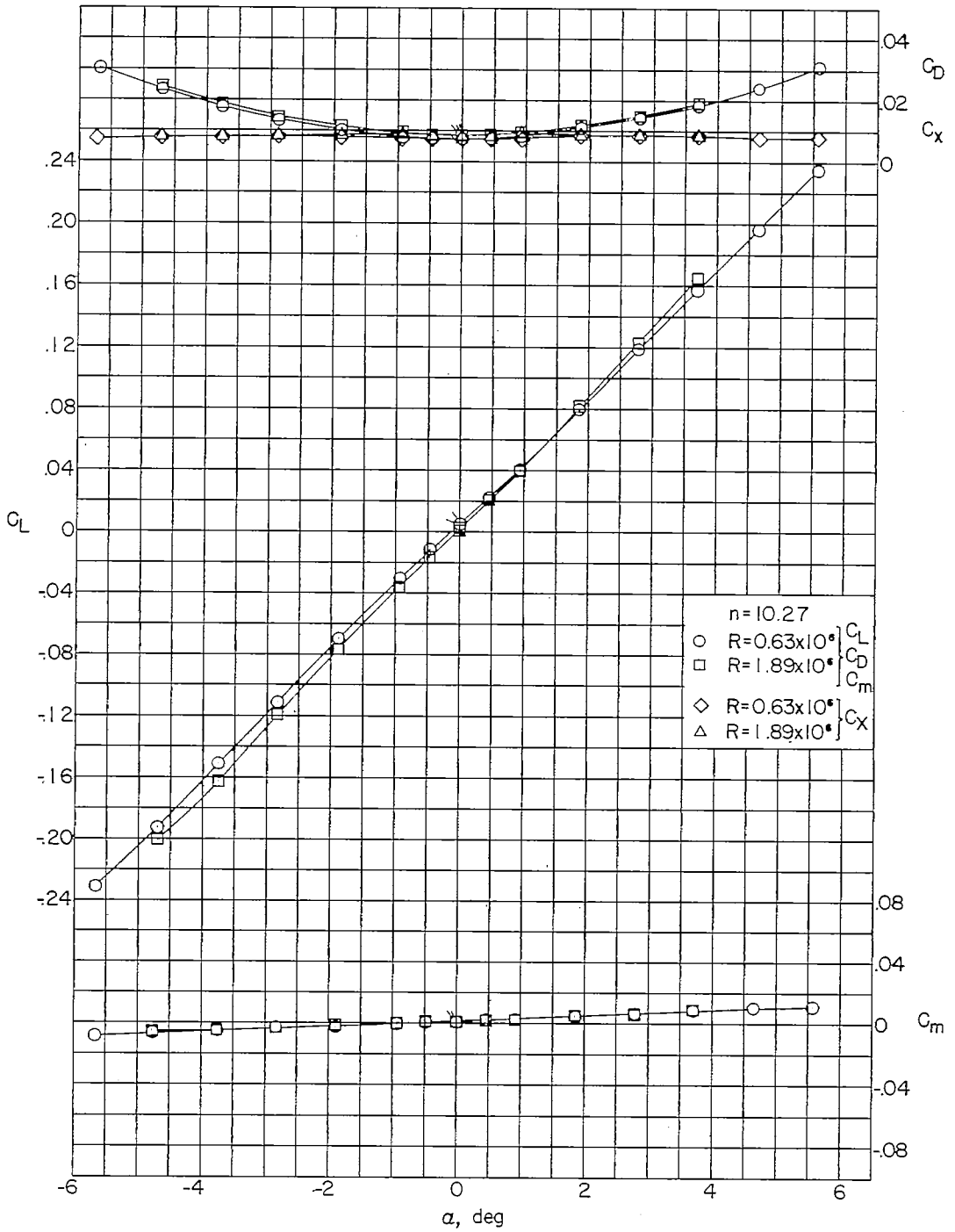

Figure 6.- Aerodynamic characteristics of the wing in the presence of the n = 10.27 body for triangular wing 2 ($\epsilon = 30^{\circ}$). Flagged symbols denote check values.

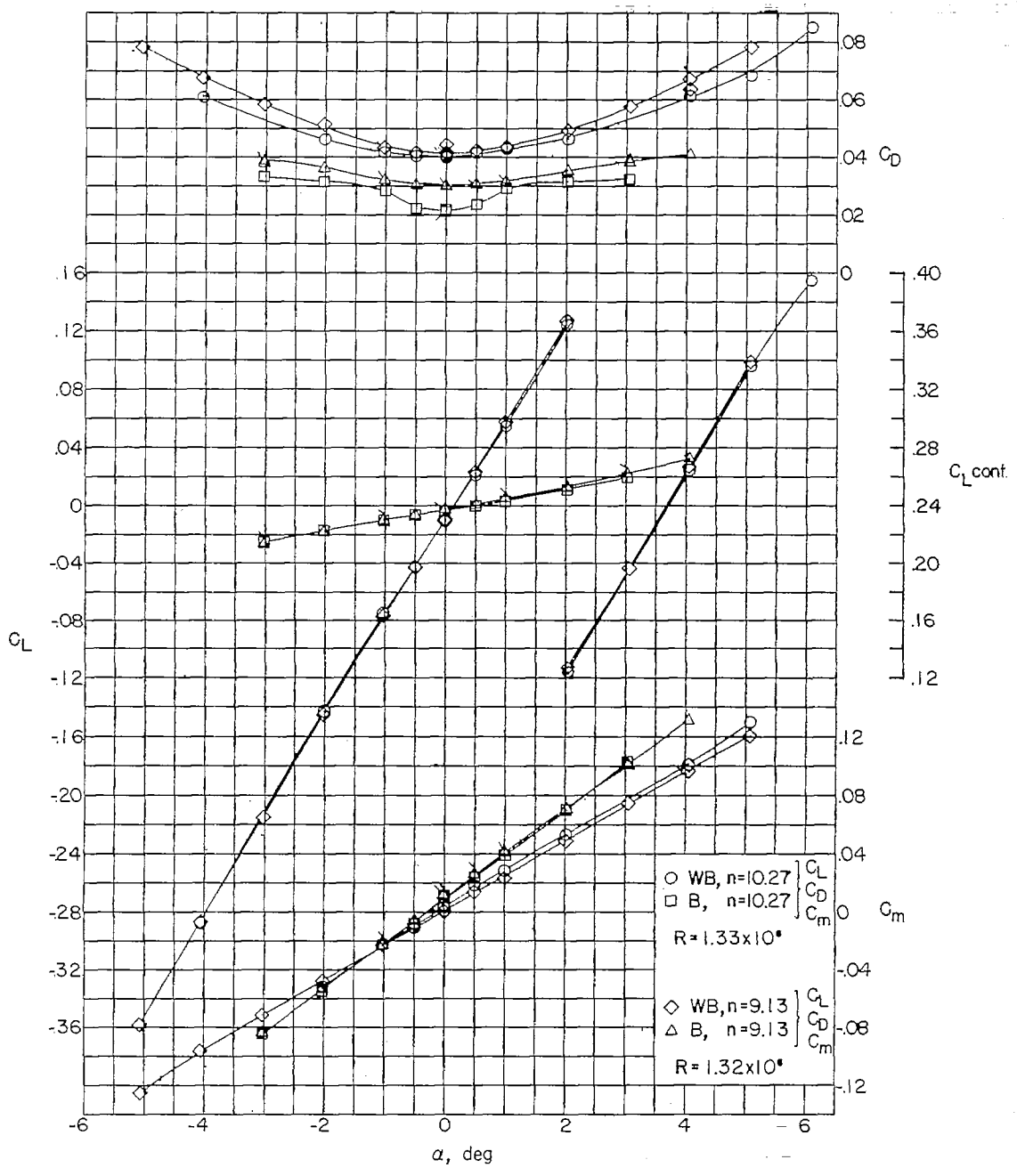

Figure 7.- Aerodynamic characteristics of the wing and body combination for triangular wing 3 ($\epsilon = 30^\circ$) and the n = 10.27 and n = 9.13 bodies alone. (Body-alone results are based on exposed area of triangular wing 3.) Flagged symbols denote check values.

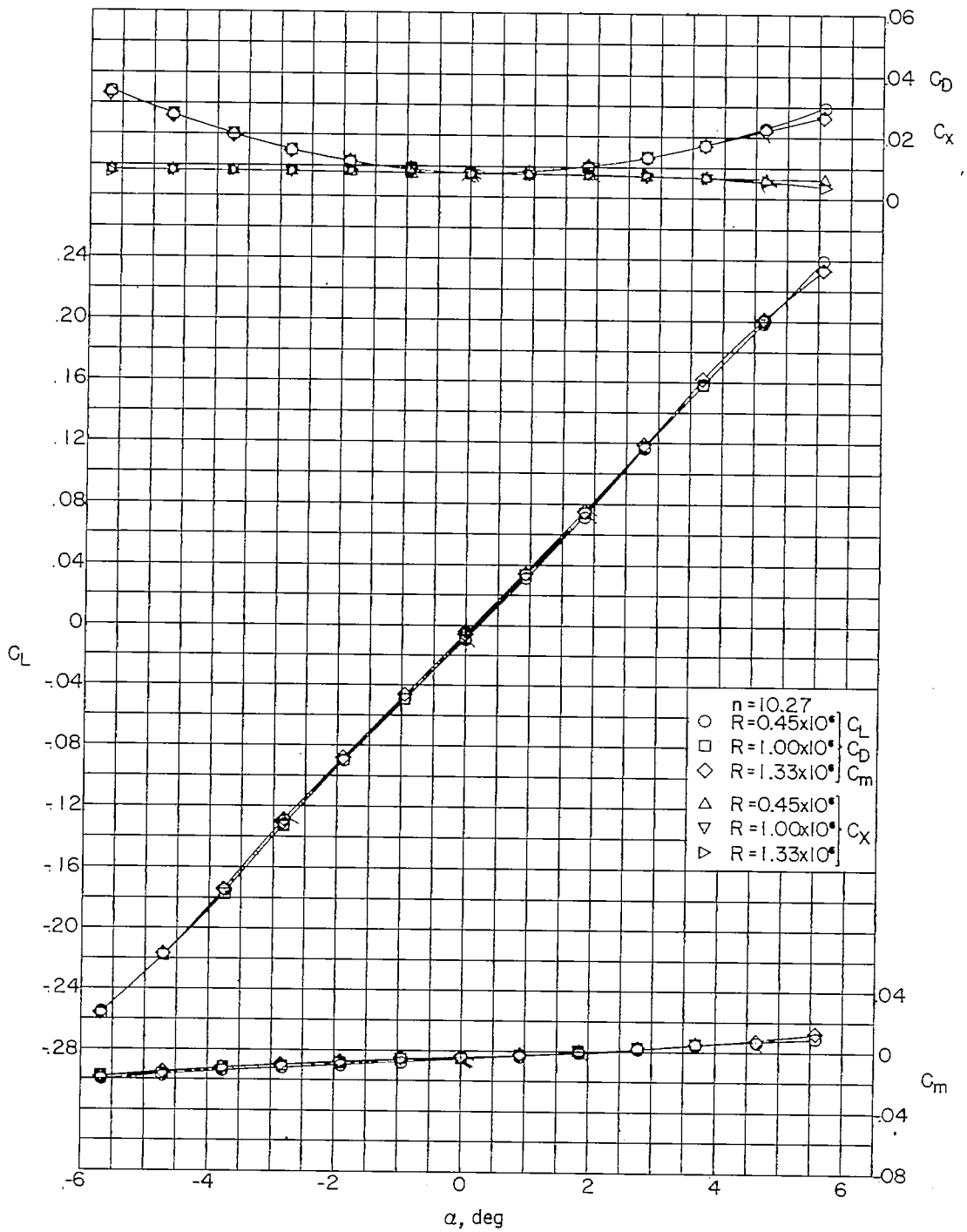

Figure 8.- Aerodynamic characteristics of the wing in the presence of the n = 10.27 body for triangular wing 3 ($\epsilon = 30^{\circ}$). Flagged symbols denote check values.

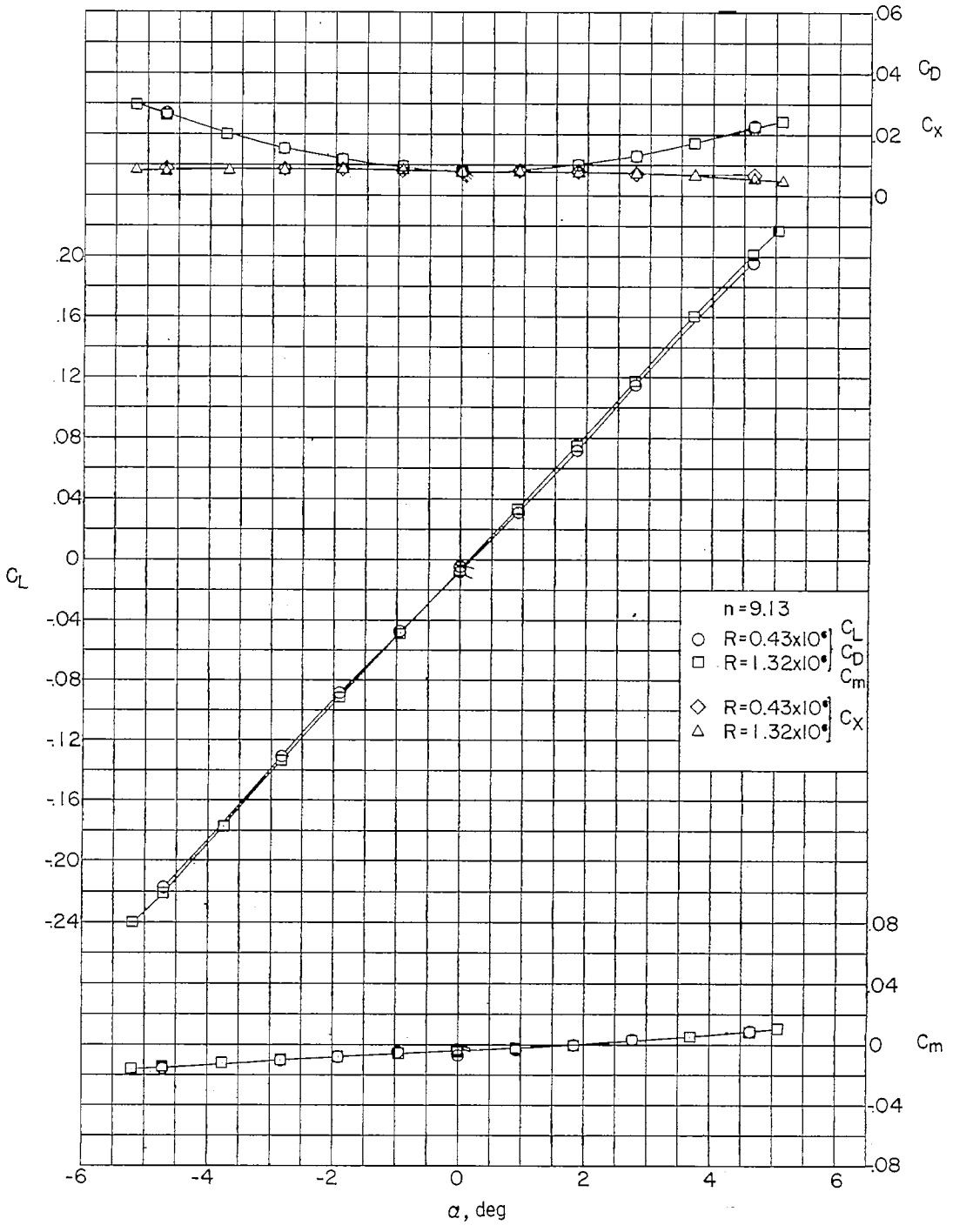

Figure 9.- Aerodynamic characteristics of the wing in the presence of the n = 9.13 body for triangular wing 3 ($\epsilon = 30^{\circ}$). Flagged symbols denote check values.

[redacted]

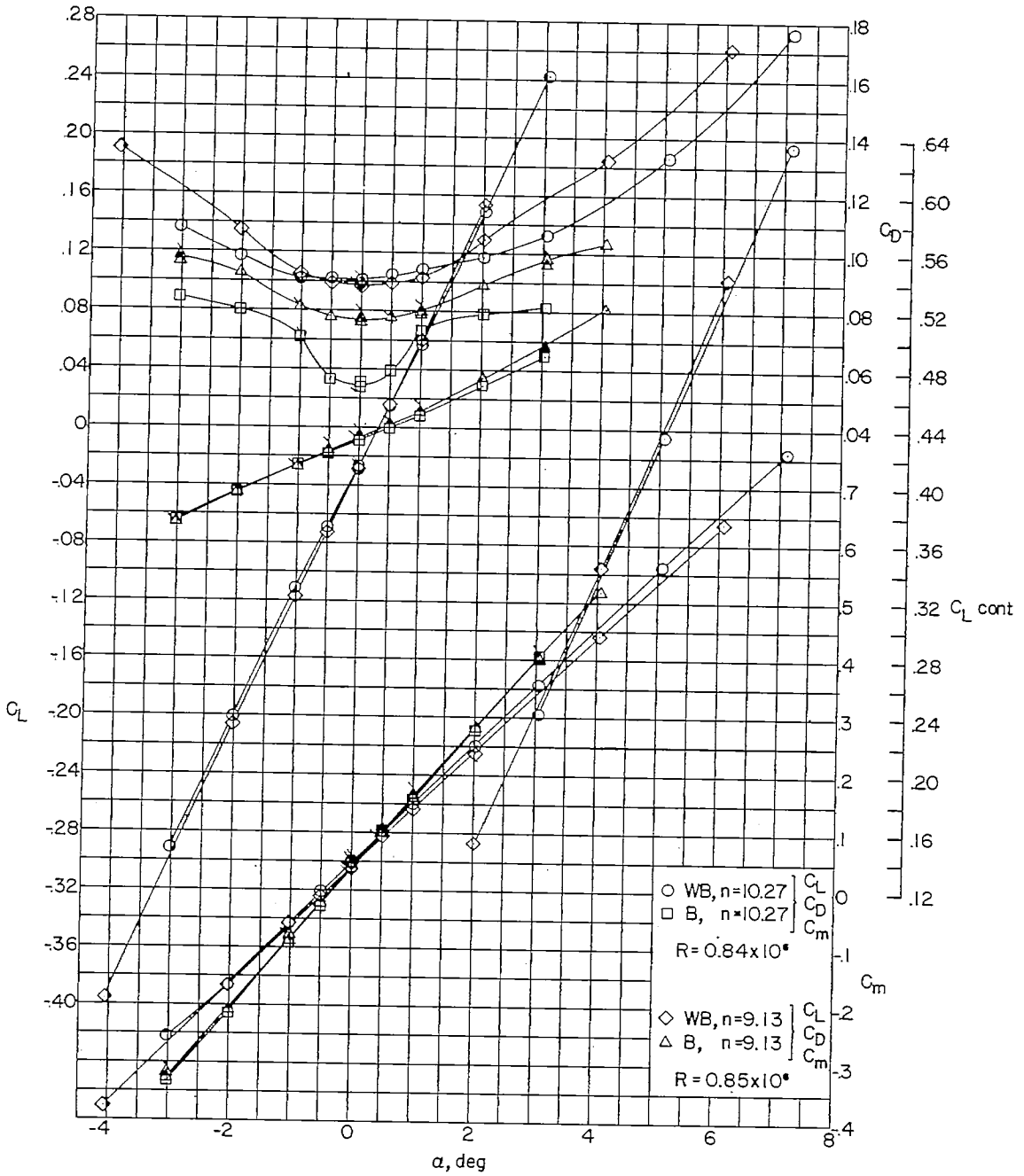

Figure 10.- Aerodynamic characteristics of the wing and body combination for triangular wing 4 ($\epsilon = 30^{\circ}$) and the n = 10.27 and n = 9.13 bodies alone. (Body-alone results are based on exposed area of triangular wing 4.) Flagged symbols denote check values.

[redacted]

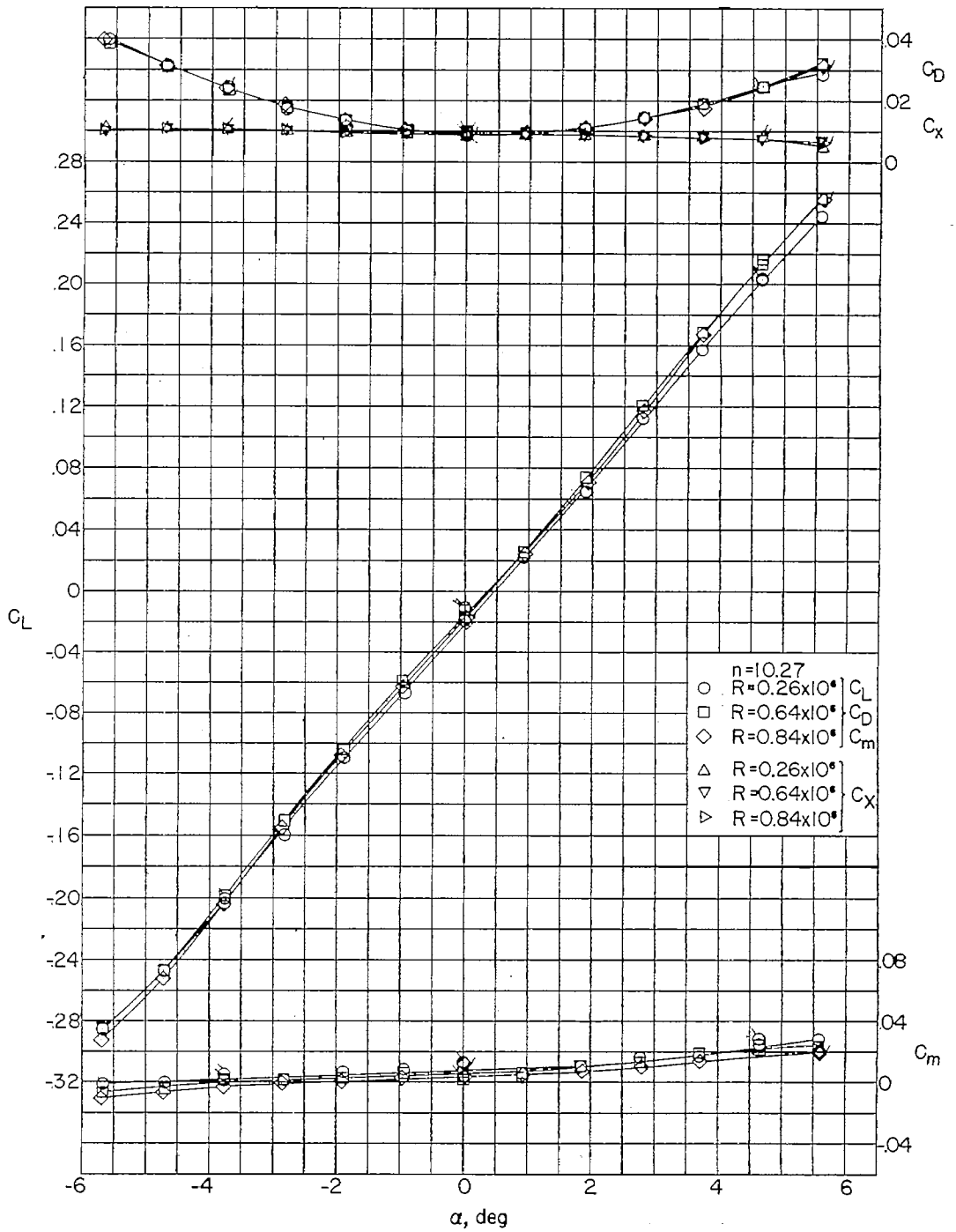

Figure 11.- Aerodynamic characteristics of the wing in the presence of the n = 10.27 body for triangular wing 4 ($\epsilon = 30^{\circ}$). Flagged symbols denote check values.

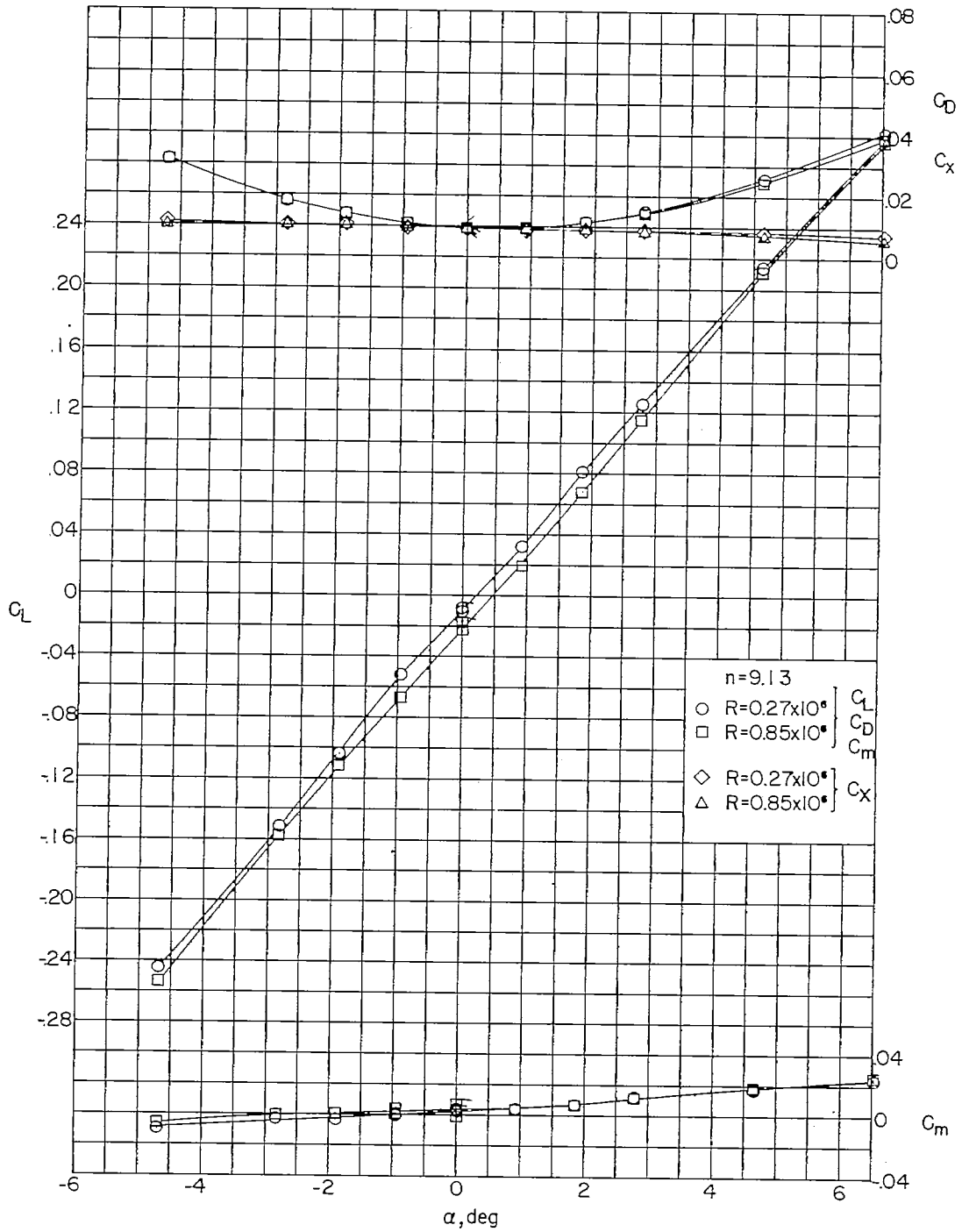

Figure 12.- Aerodynamic characteristics of the wing in the presence of the n = 9.13 body for triangular wing 4 ($\epsilon = 30^{\circ}$). Flagged symbols denote check values.

[redacted]

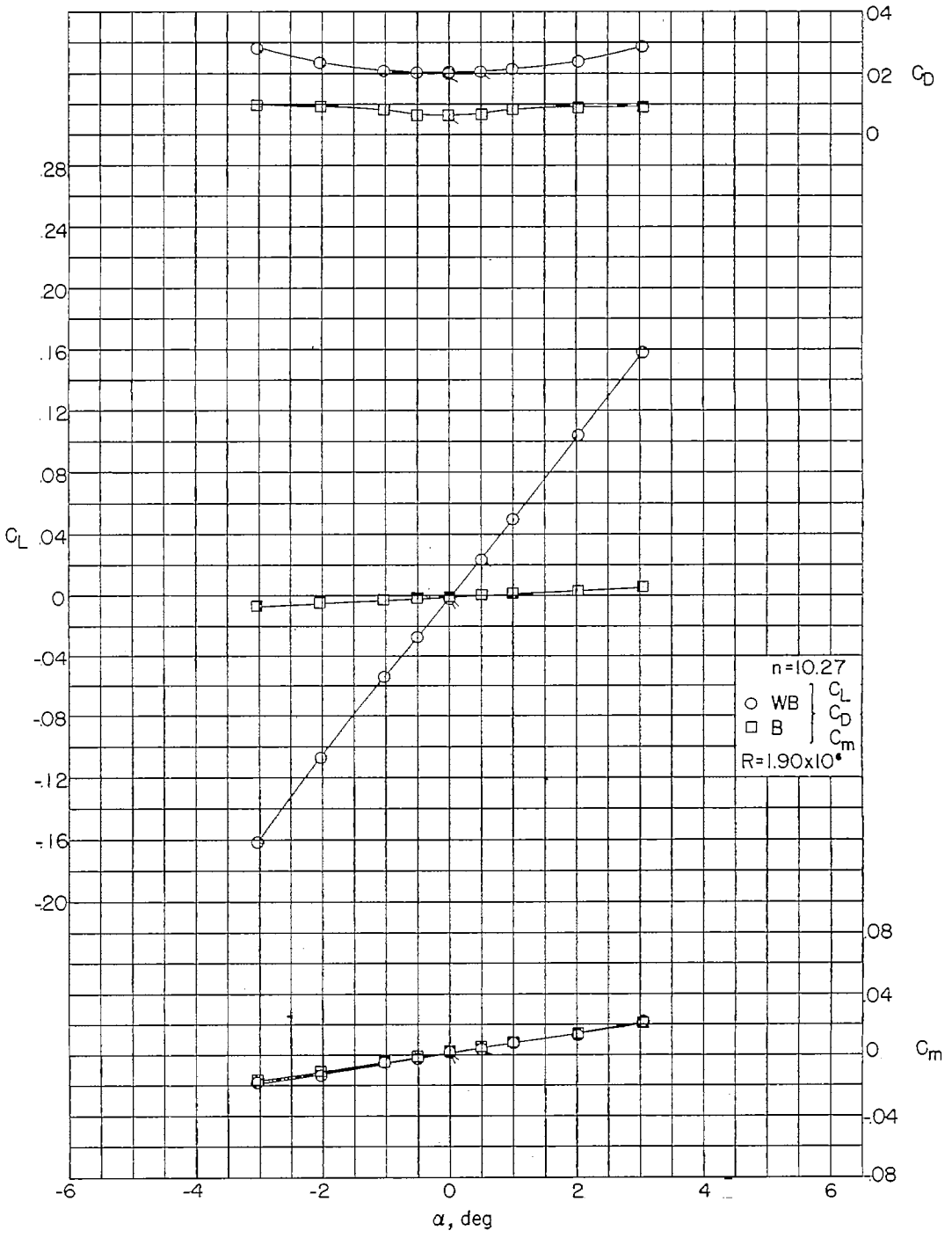

Figure 13.- Aerodynamic characteristics of the wing and body combination for triangular wing 5 ($\epsilon = 45^\circ$) and the n = 10.27 body alone. (Body-alone results are based on exposed area of triangular wing 5.) Flagged symbols denote check values.

[redacted]

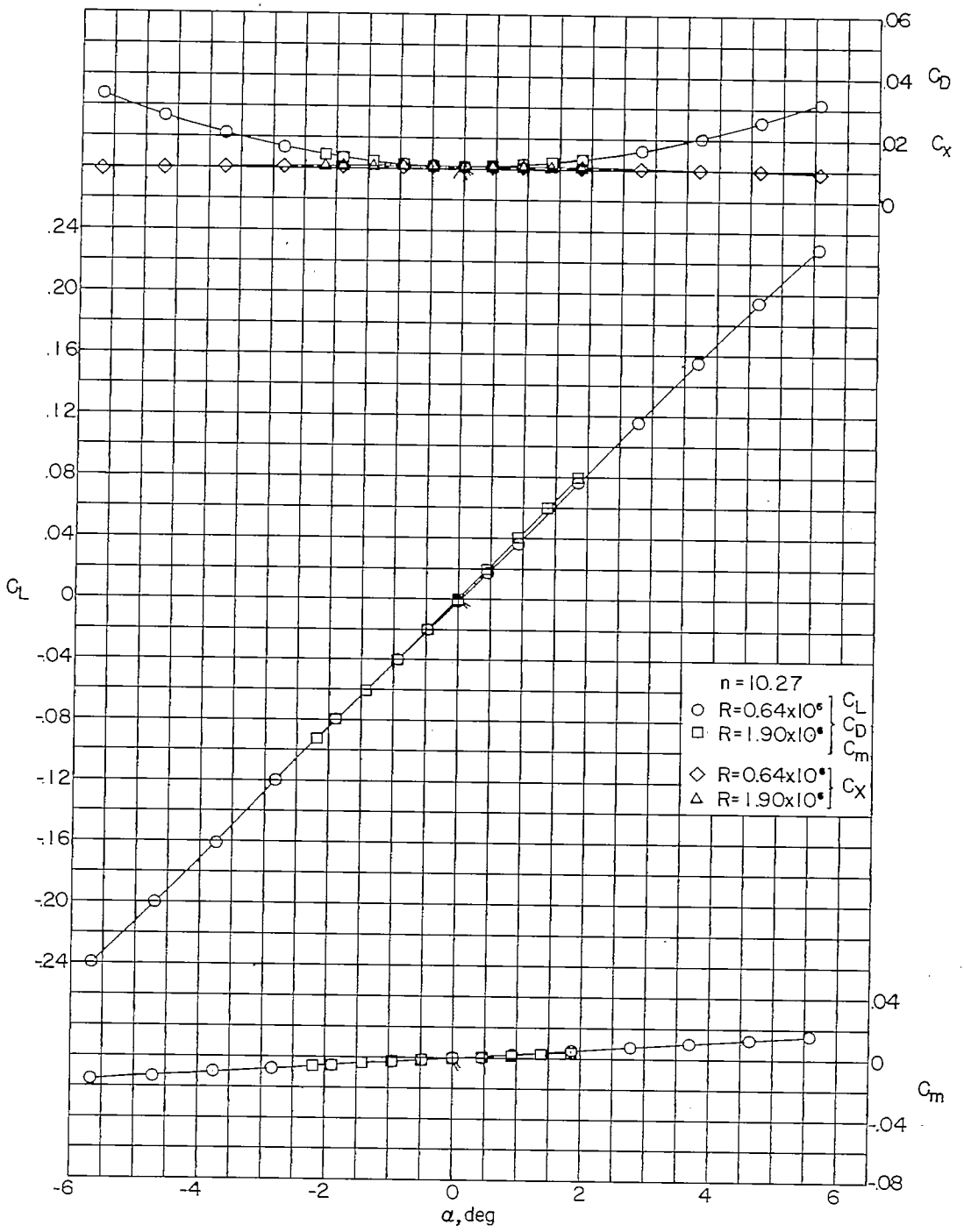

Figure 14.- Aerodynamic characteristics of the wing in the presence of the n = 10.27 body for triangular wing 5 ($\epsilon = 45^\circ$). Flagged symbols denote check values.

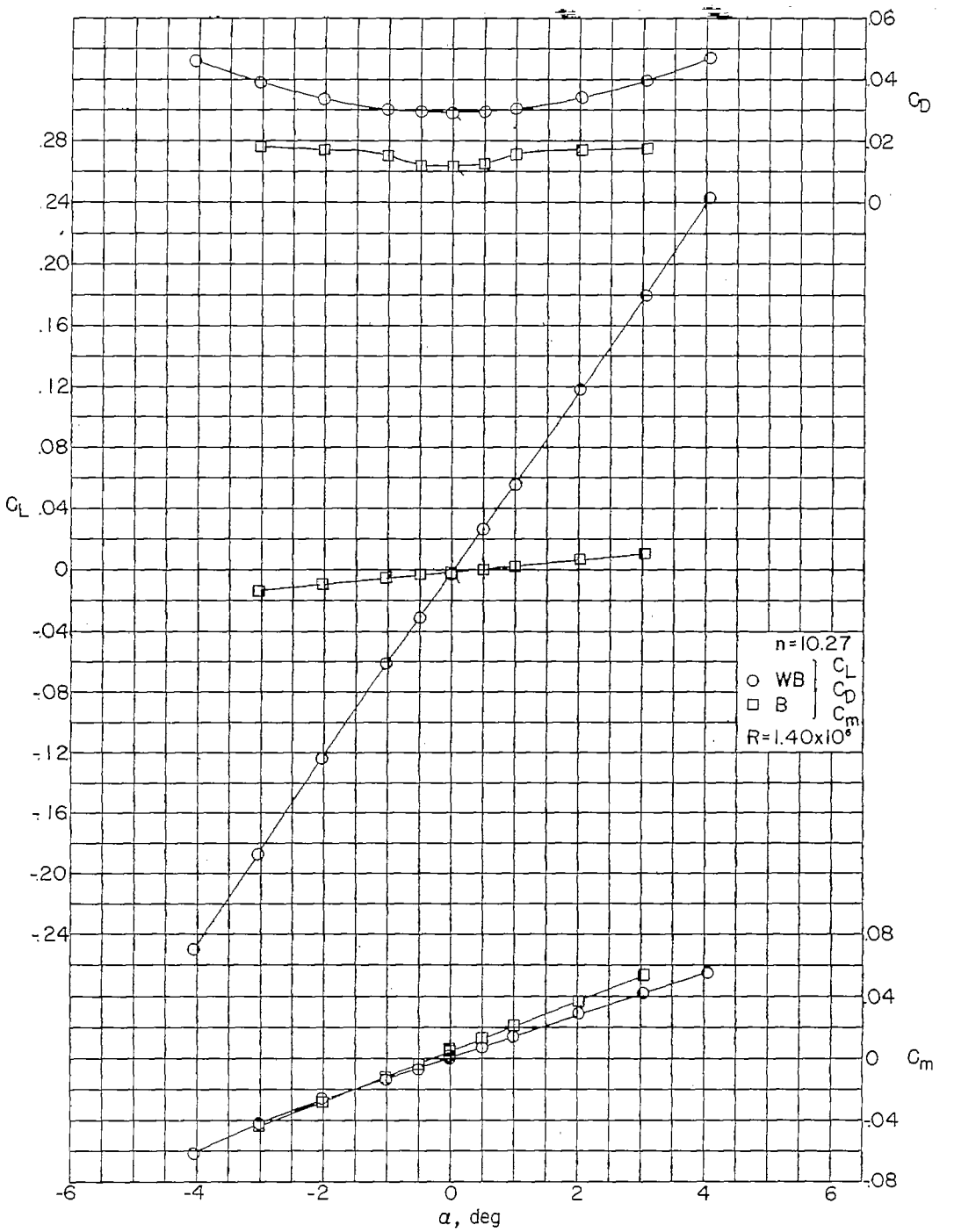

Figure 15.- Aerodynamic characteristics of the wing and body combination for triangular wing 6 ($\epsilon = 45^\circ$) and the n = 10.27 body alone. (Body-alone results are based on exposed area of triangular wing 6.) Flagged symbols denote check values.

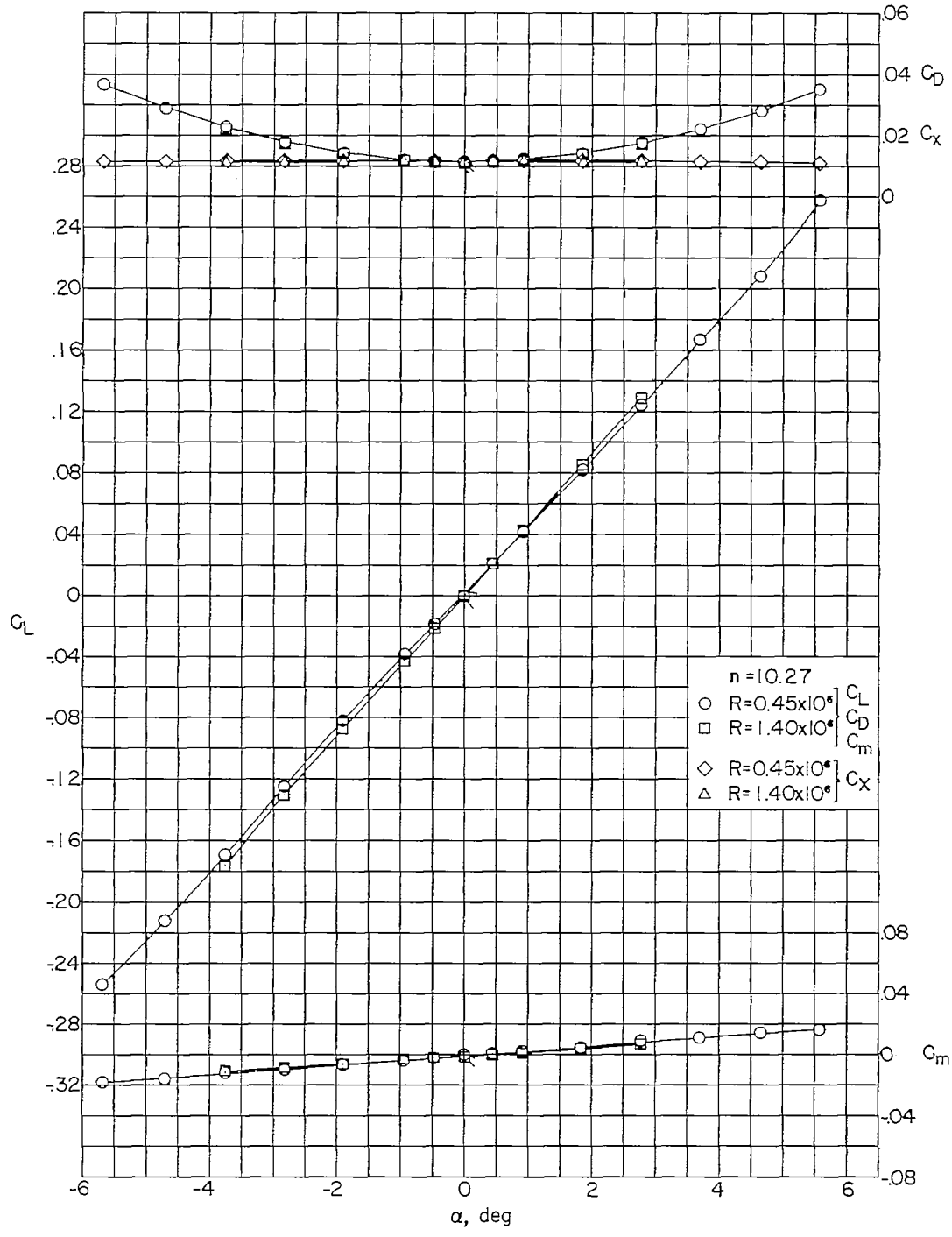

Figure 16.- Aerodynamic characteristics of the wing in the presence of the n = 10.27 body for triangular wing 6 ($\epsilon = 45^{\circ}$). Flagged symbols denote check values.

[redacted]

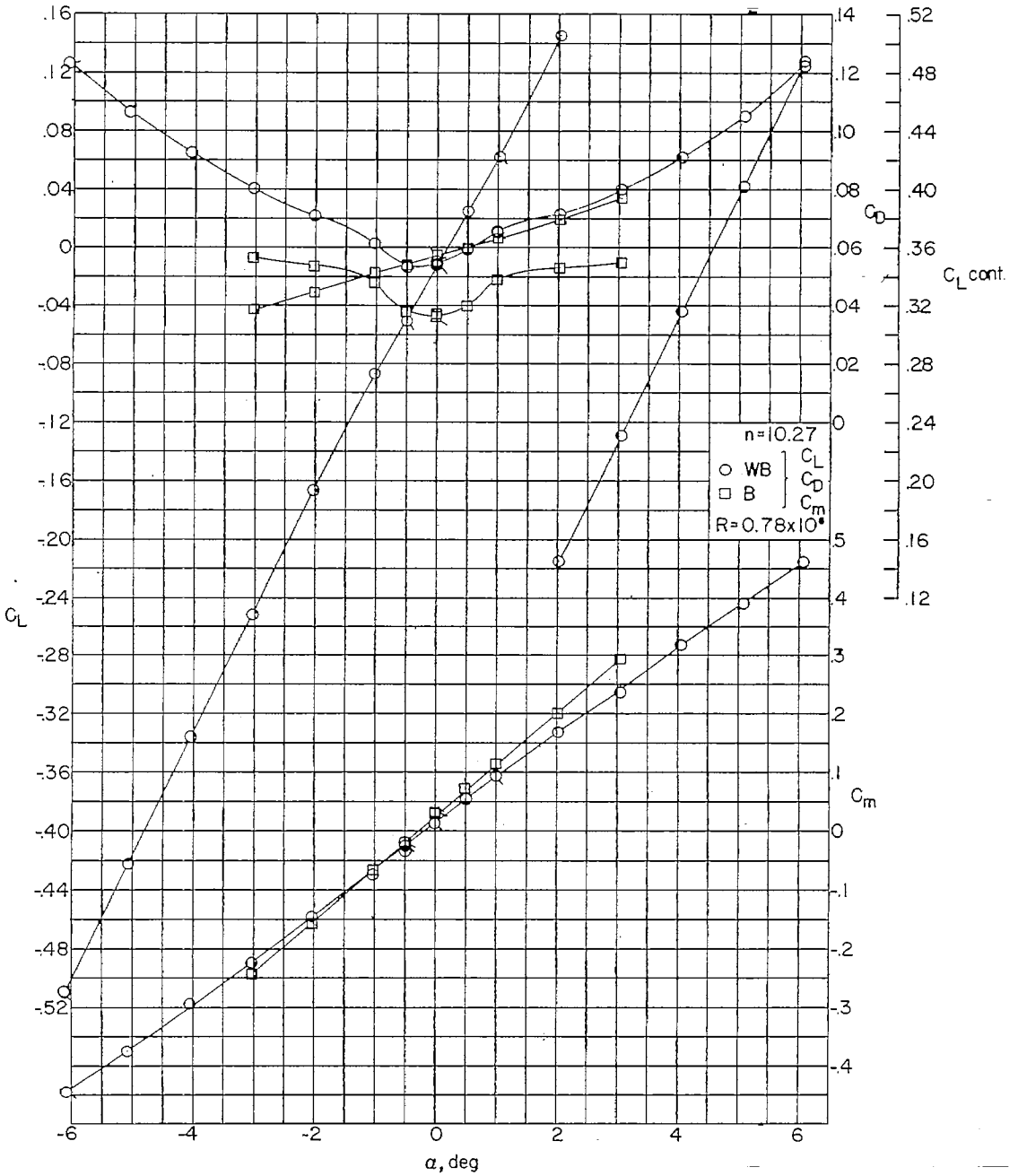

Figure 17.- Aerodynamic characteristics of the wing and body combination for triangular wing 7 ($\epsilon = 45^{\circ}$) and the n = 10.27 body alone. (Body-alone results are based on exposed area of triangular wing 7.) Flagged symbols denote check values.

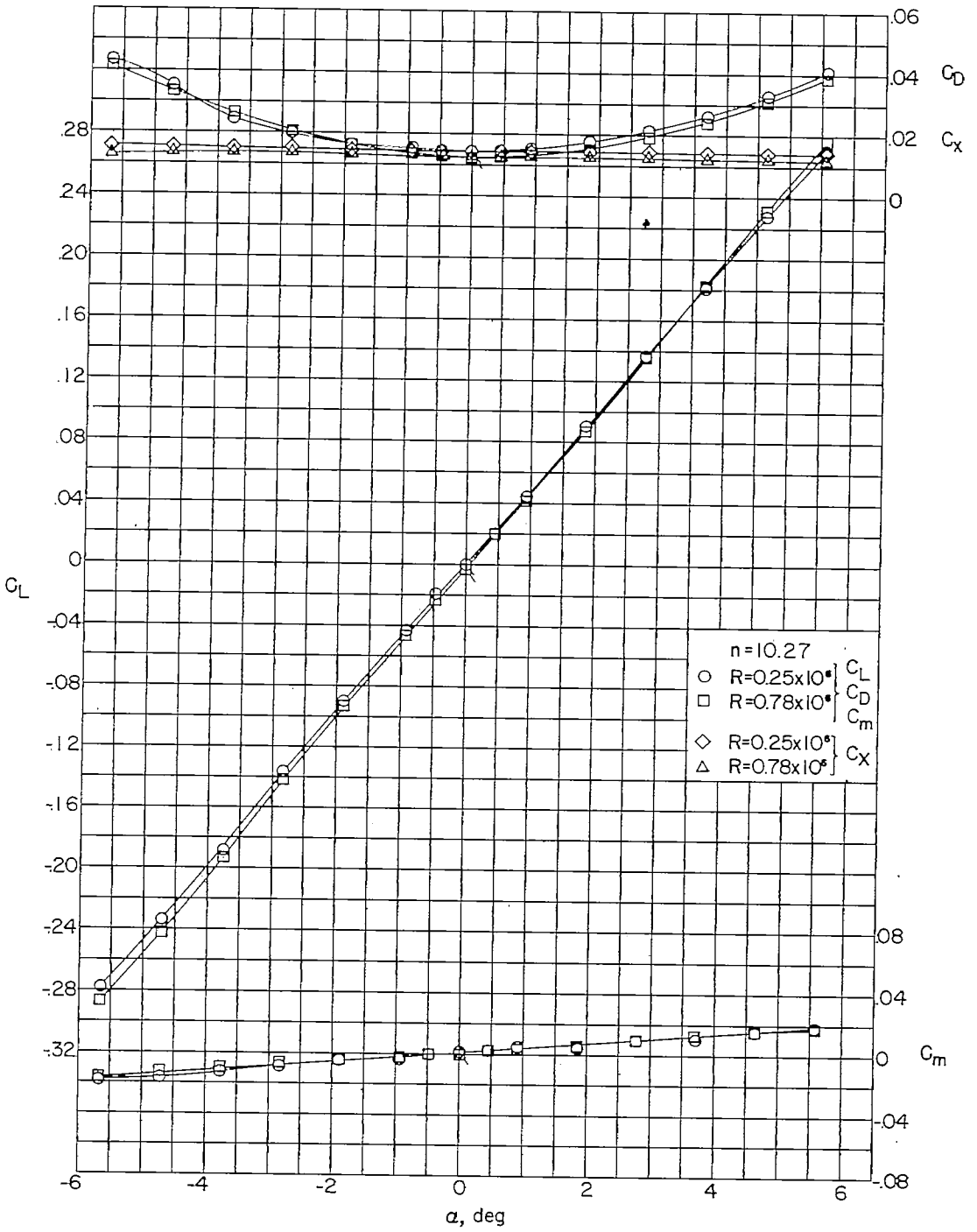

Figure 18.- Aerodynamic characteristics of the wing in the presence of the n = 10.27 body for triangular wing 7 ($\epsilon = 45^{\circ}$). Flagged symbols denote check values.

[redacted]

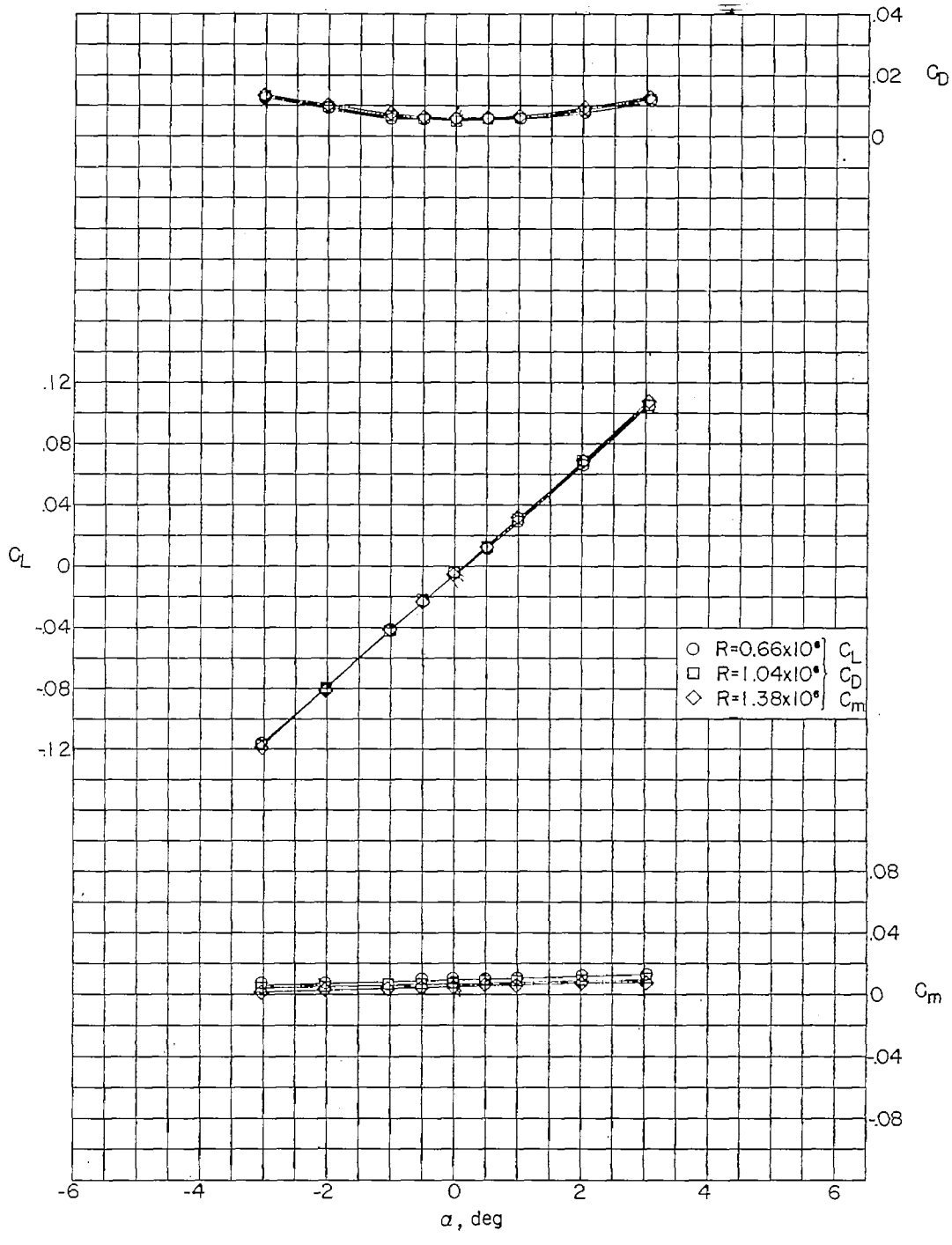

Figure 19.- Aerodynamic characteristics of triangular wing 2 ($\epsilon = 30^{\circ}$) alone. Flagged symbols denote check values.

[redacted]

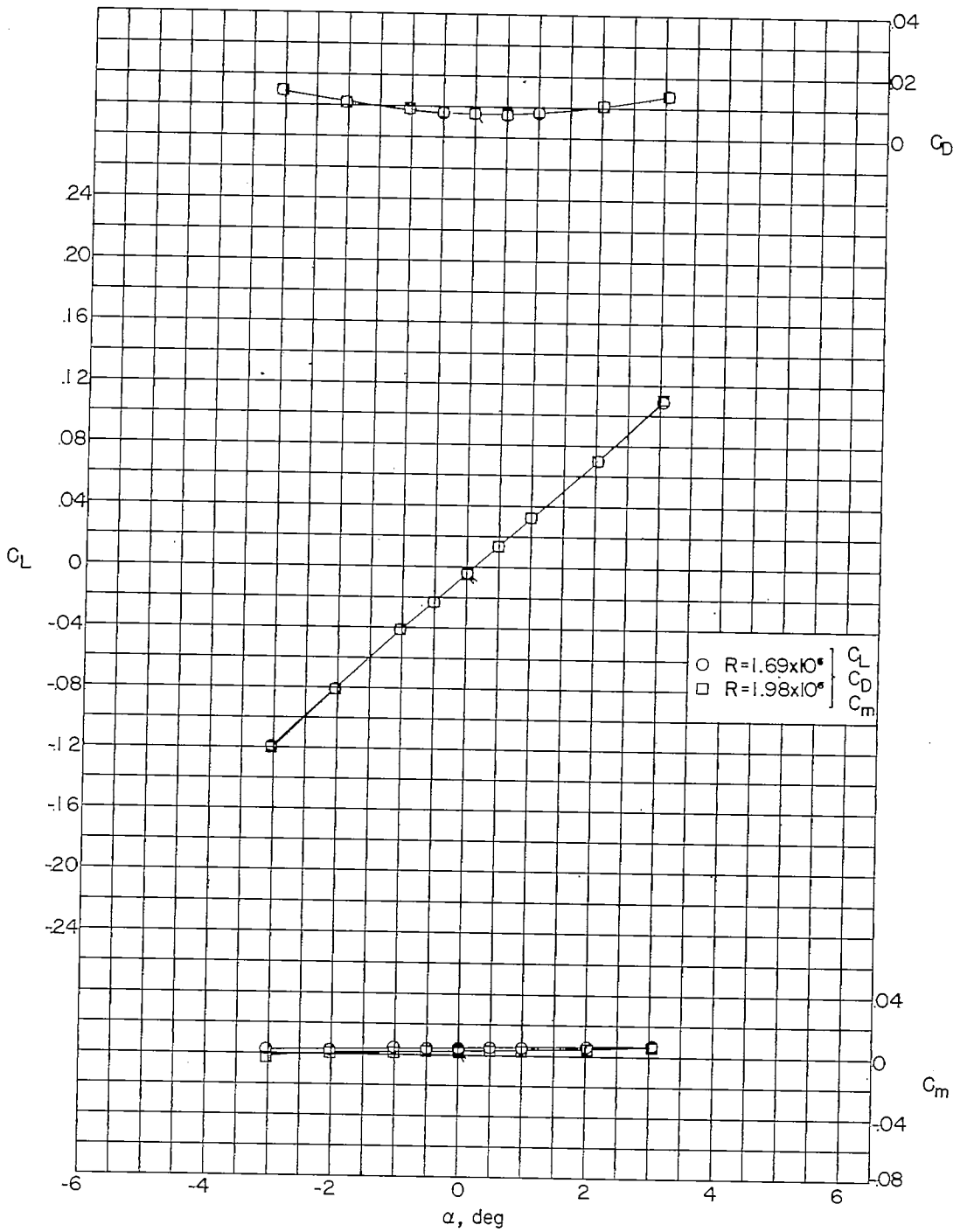

Figure 19.- Concluded.

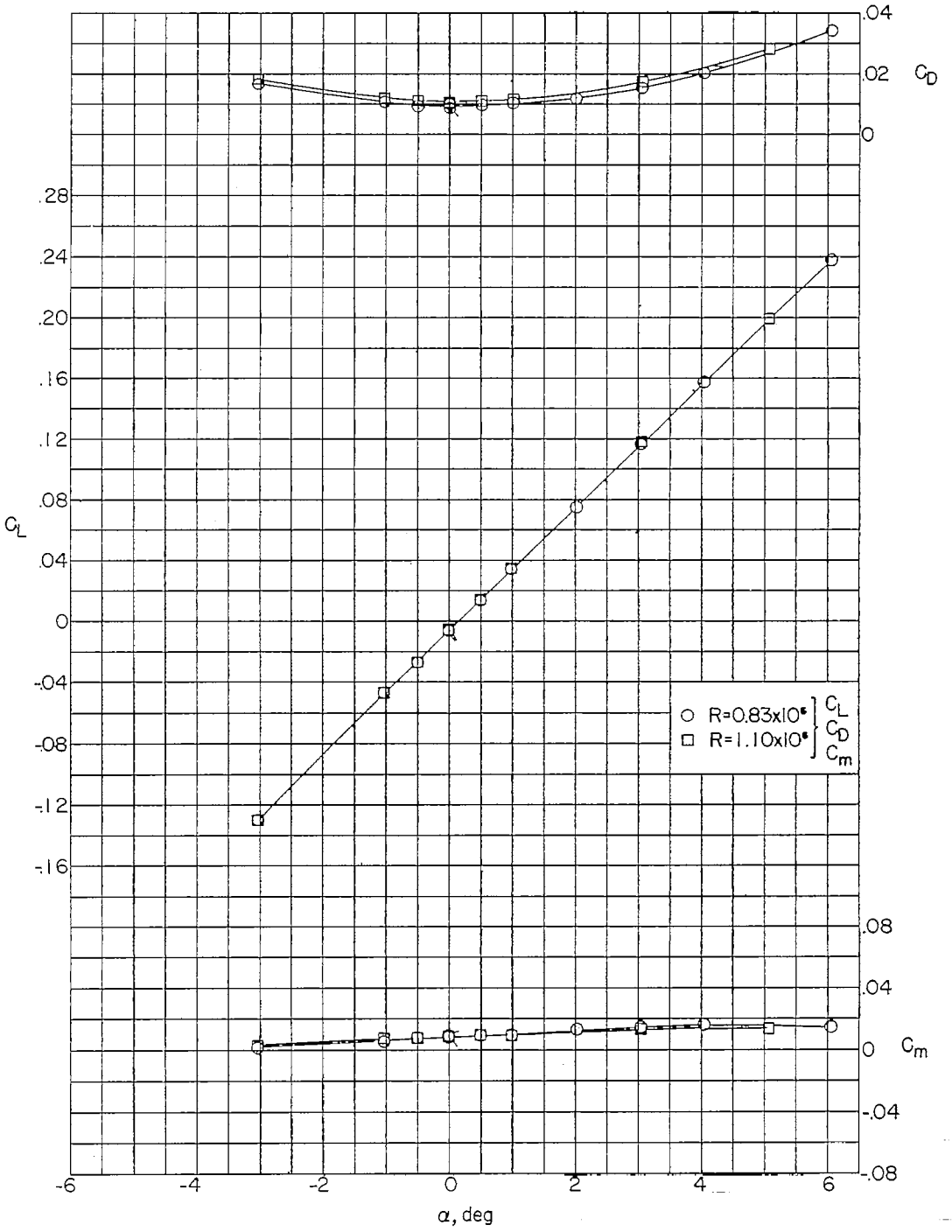

Figure 20.- Aerodynamic characteristics of triangular wing 6 ($\epsilon = 45^\circ$) alone. Flagged symbols denote check values.

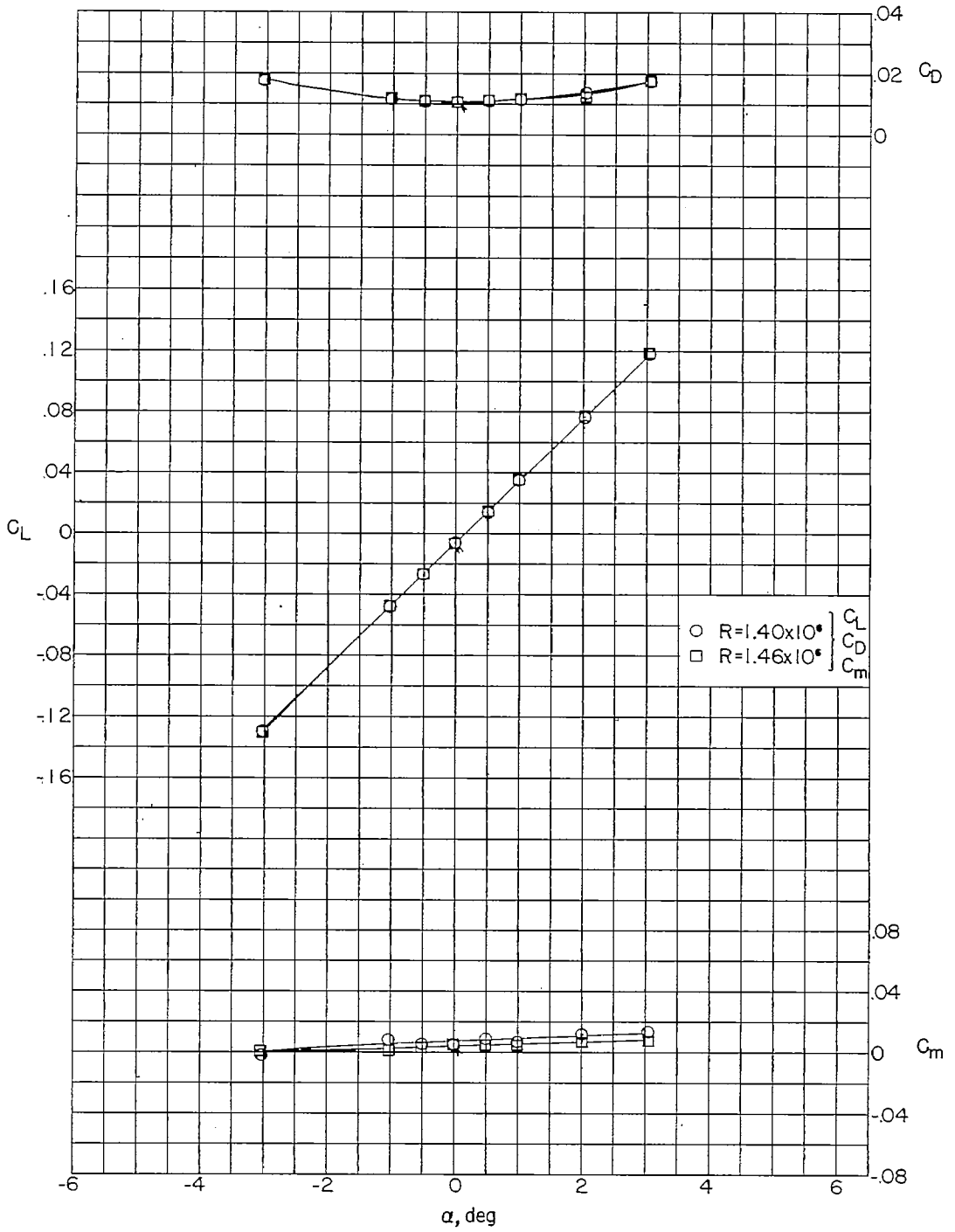

Figure 20.- Concluded.

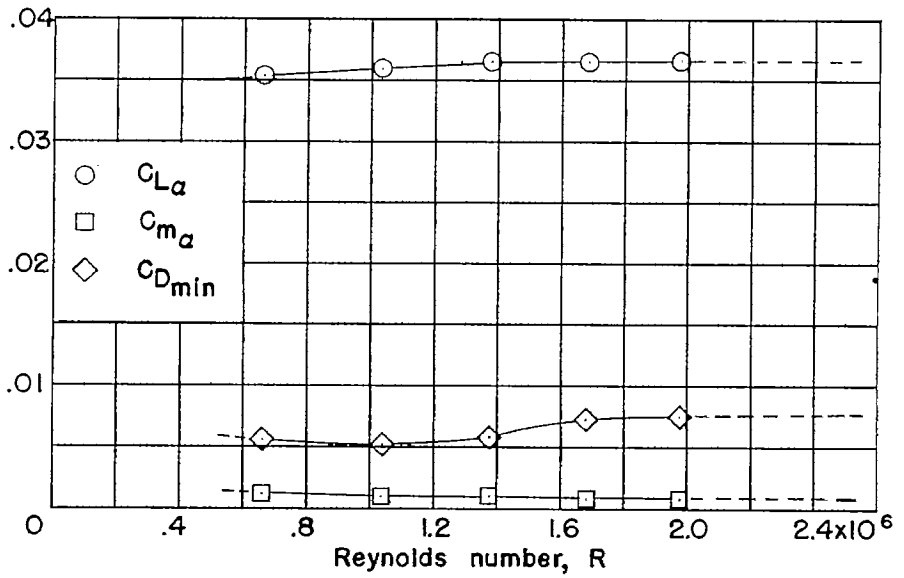

(a) Wing 2 ($\epsilon = 30^\circ$) alone.

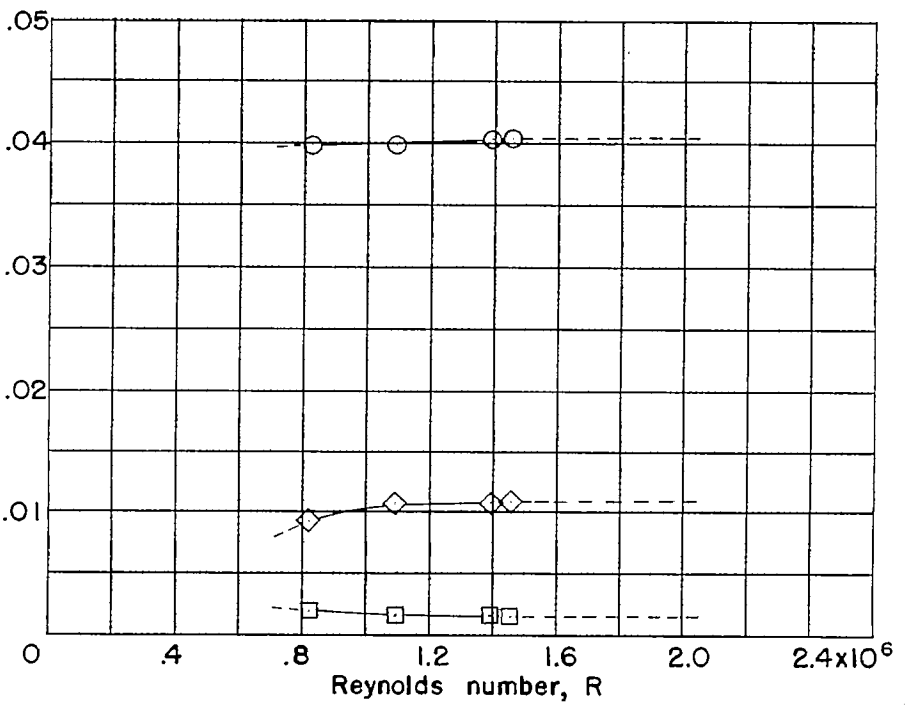

(b) Wing 6 ($\epsilon = 45^\circ$) alone.

Figure 21.- Variation of the aerodynamic characteristics of wings 2 and 6 alone as a function of Reynolds number at M = 1.94.

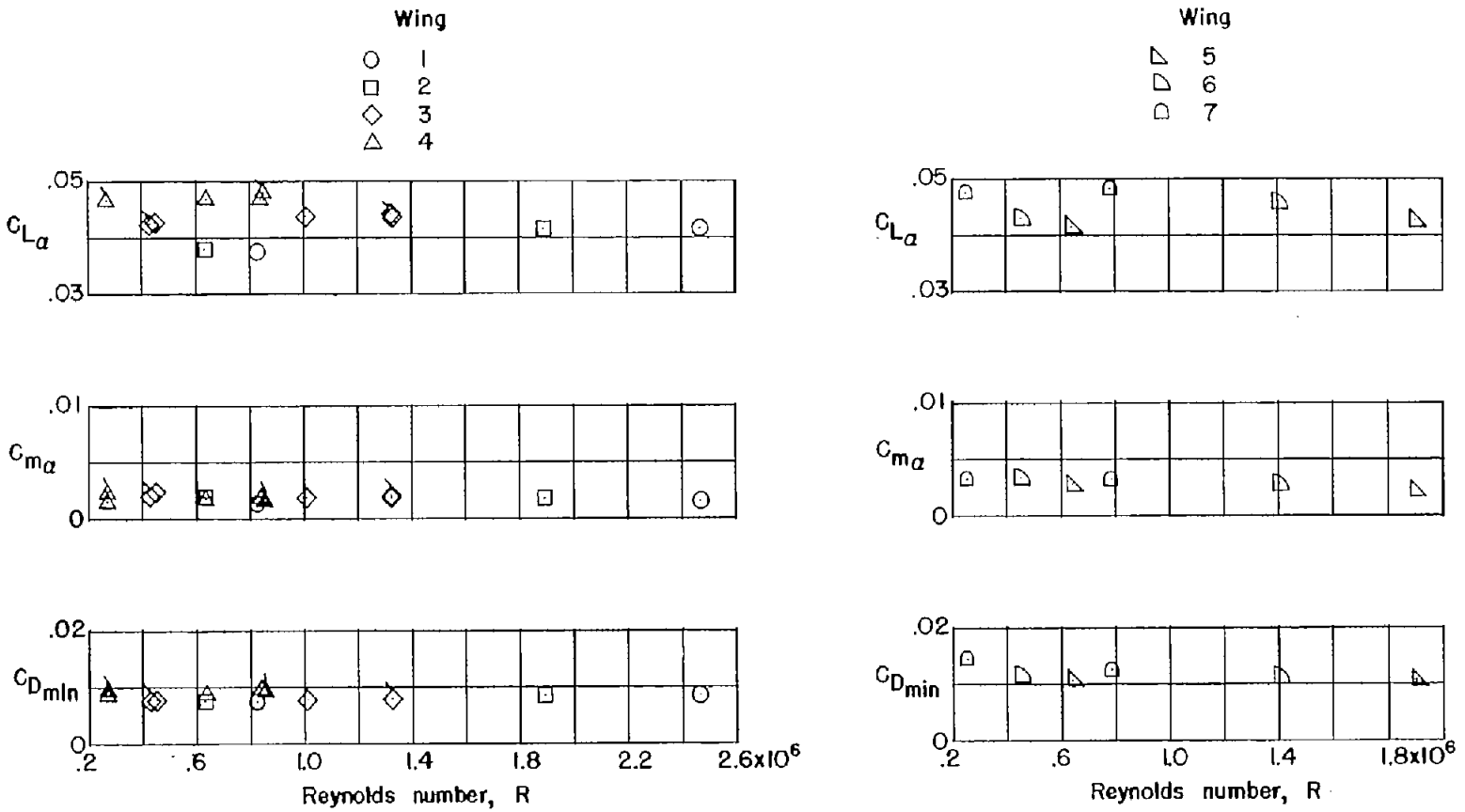

(a) $\epsilon = 30^\circ$.

(b) $\epsilon = 45^\circ$.

Figure 22.- Effect of Reynolds number on the aerodynamic characteristics of the wing in the presence of the n = 10.27 body, W(B). Flagged symbols denote n = 9.13 body.

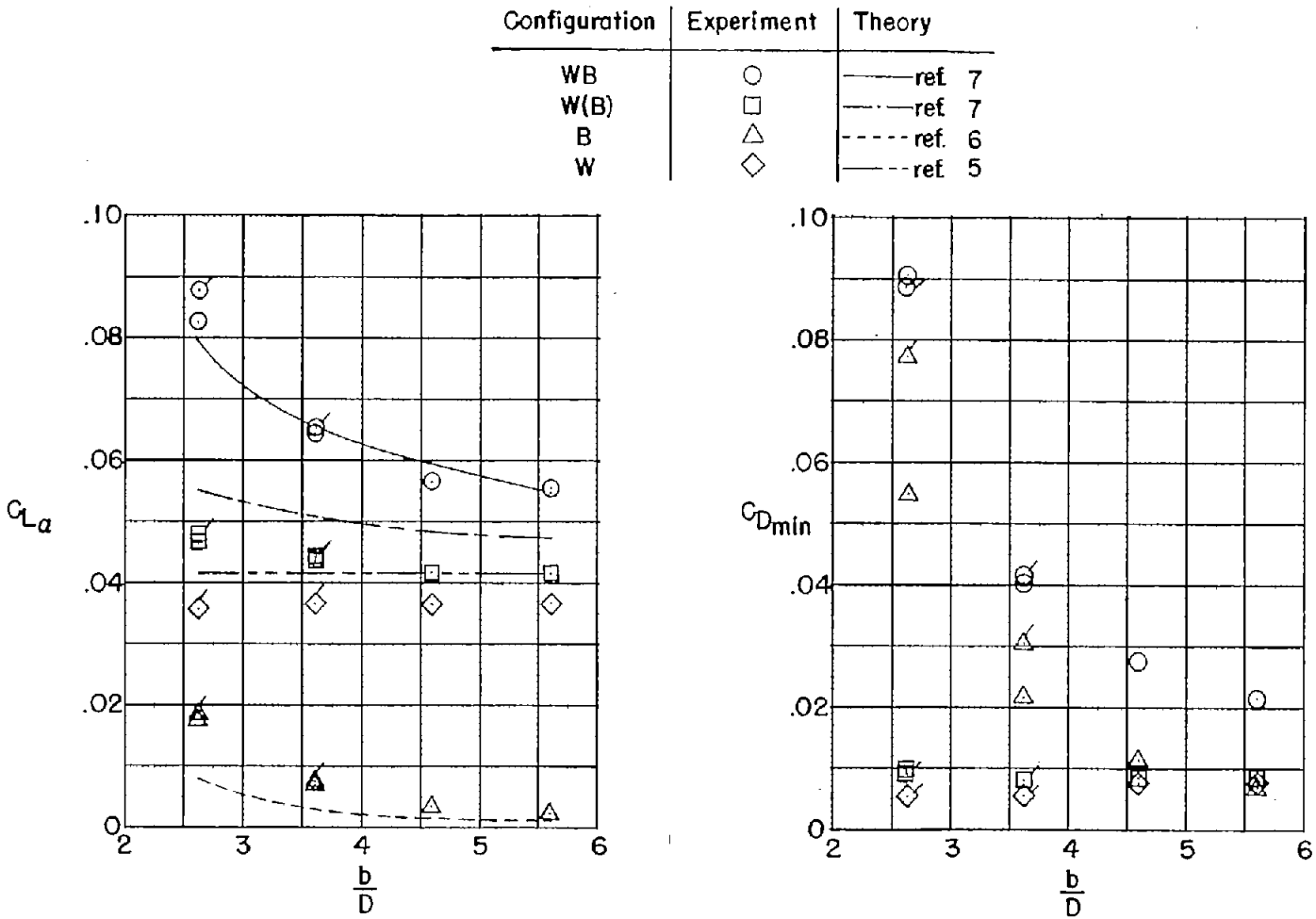

Figure 23.- Comparison of the experimental and theoretical aerodynamic characteristics of WB, W(B), W, and B for a series of $\epsilon = 30^{\circ}$ triangular wings and bodies having fineness ratios of 10.27 and 9.13 at $M = 1.94$. Flagged symbols denote $n = 9.13$ body. Wing-alone values are obtained at equivalent Reynolds numbers.

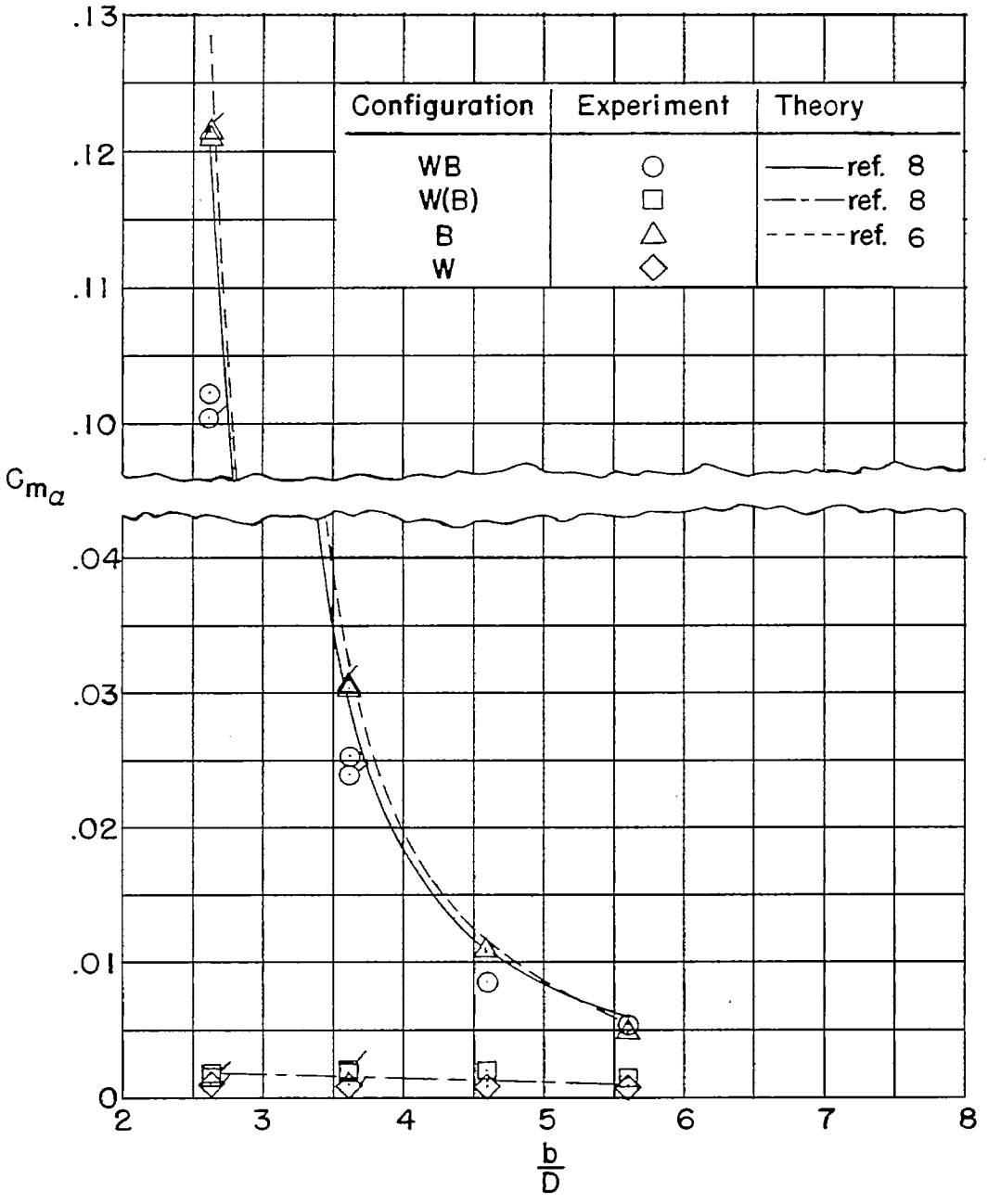

Figure 23.- Concluded.

[redacted]

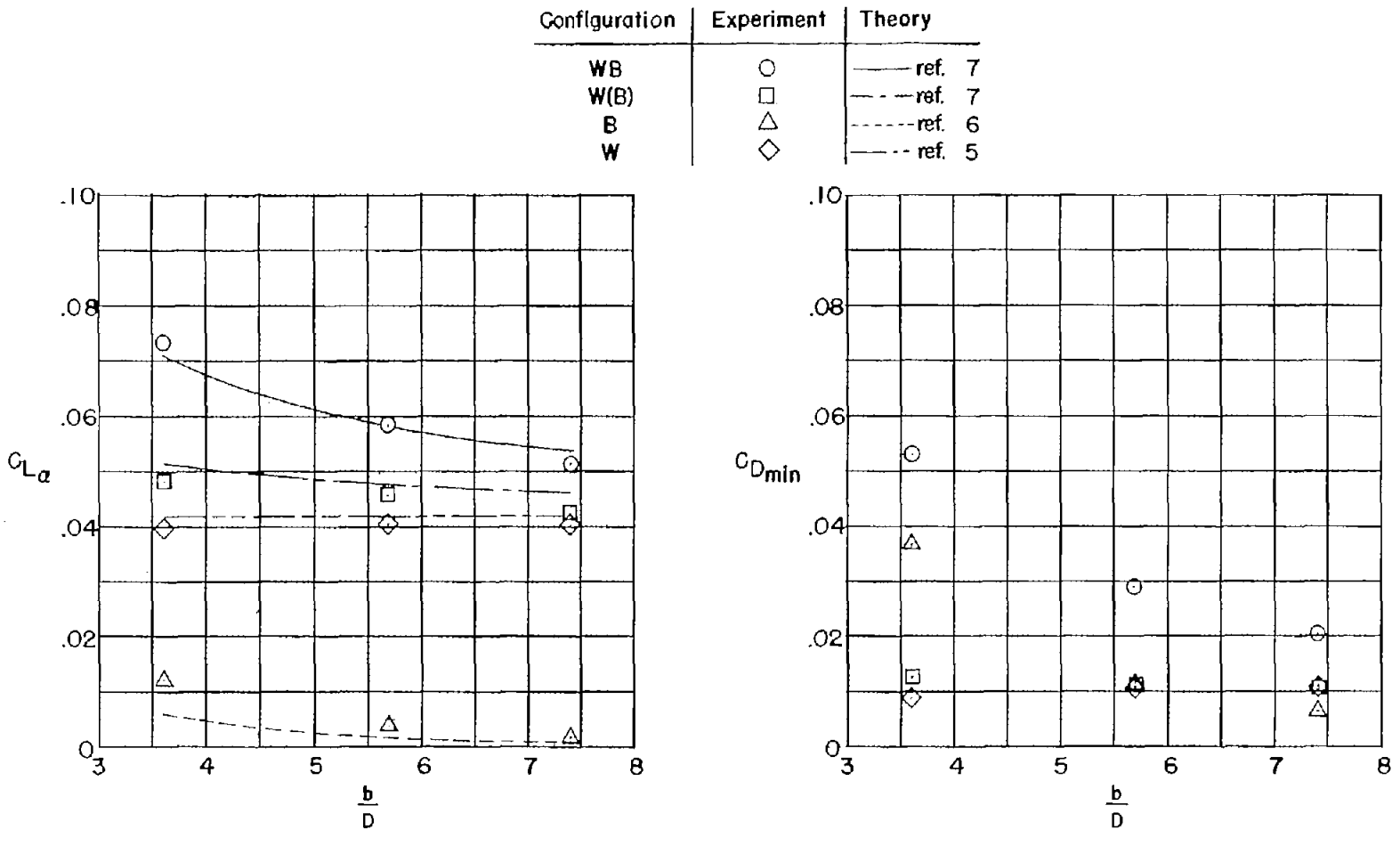

Figure 24.- Comparison of the experimental and theoretical aerodynamic characteristics of WB, W(B), W, and B for an n = 10.27 body and a series of $\epsilon = 45^\circ$ triangular wings at M = 1.94. Wing-alone values are obtained at equivalent Reynolds numbers.

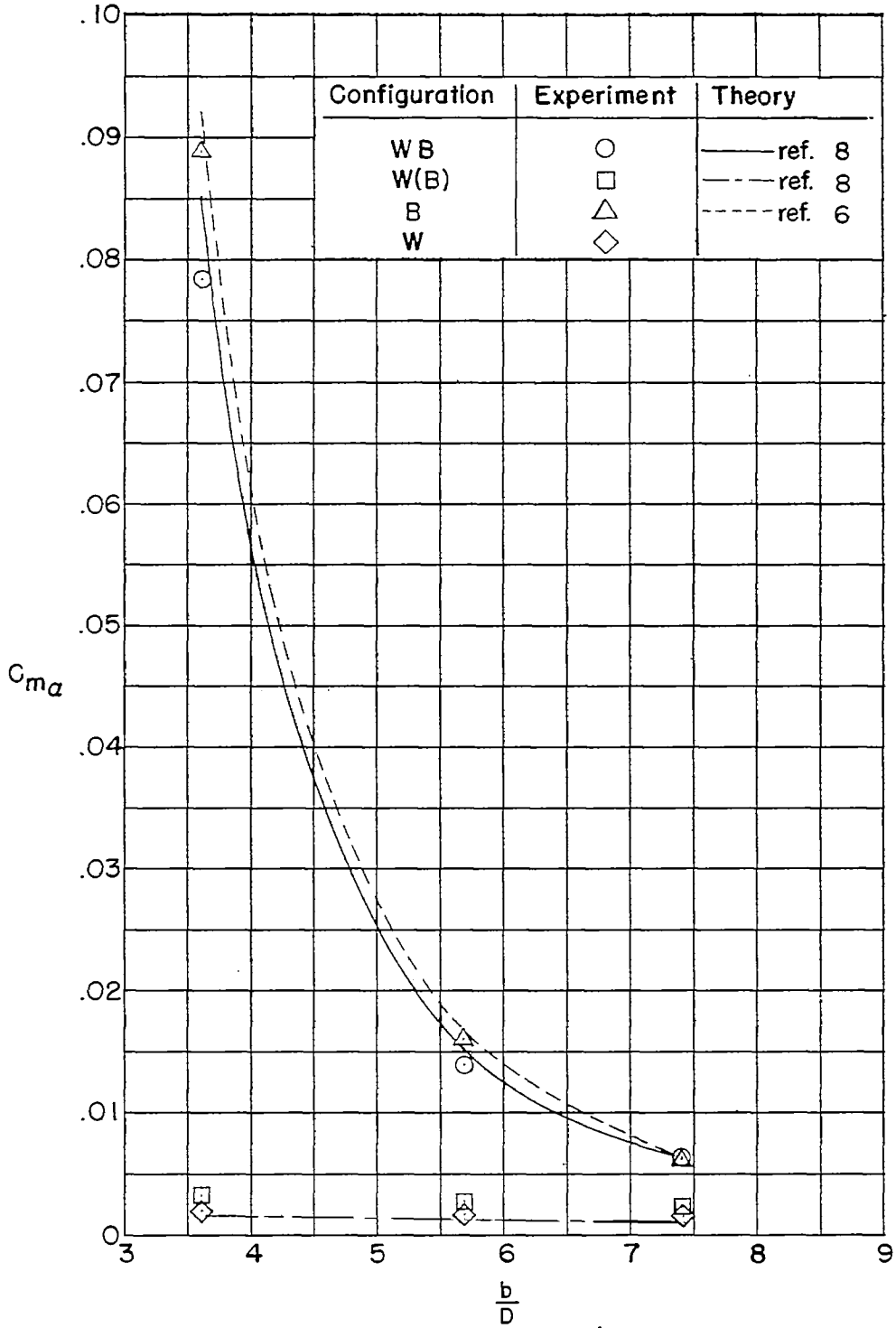

Figure 24.- Concluded.

[redacted]

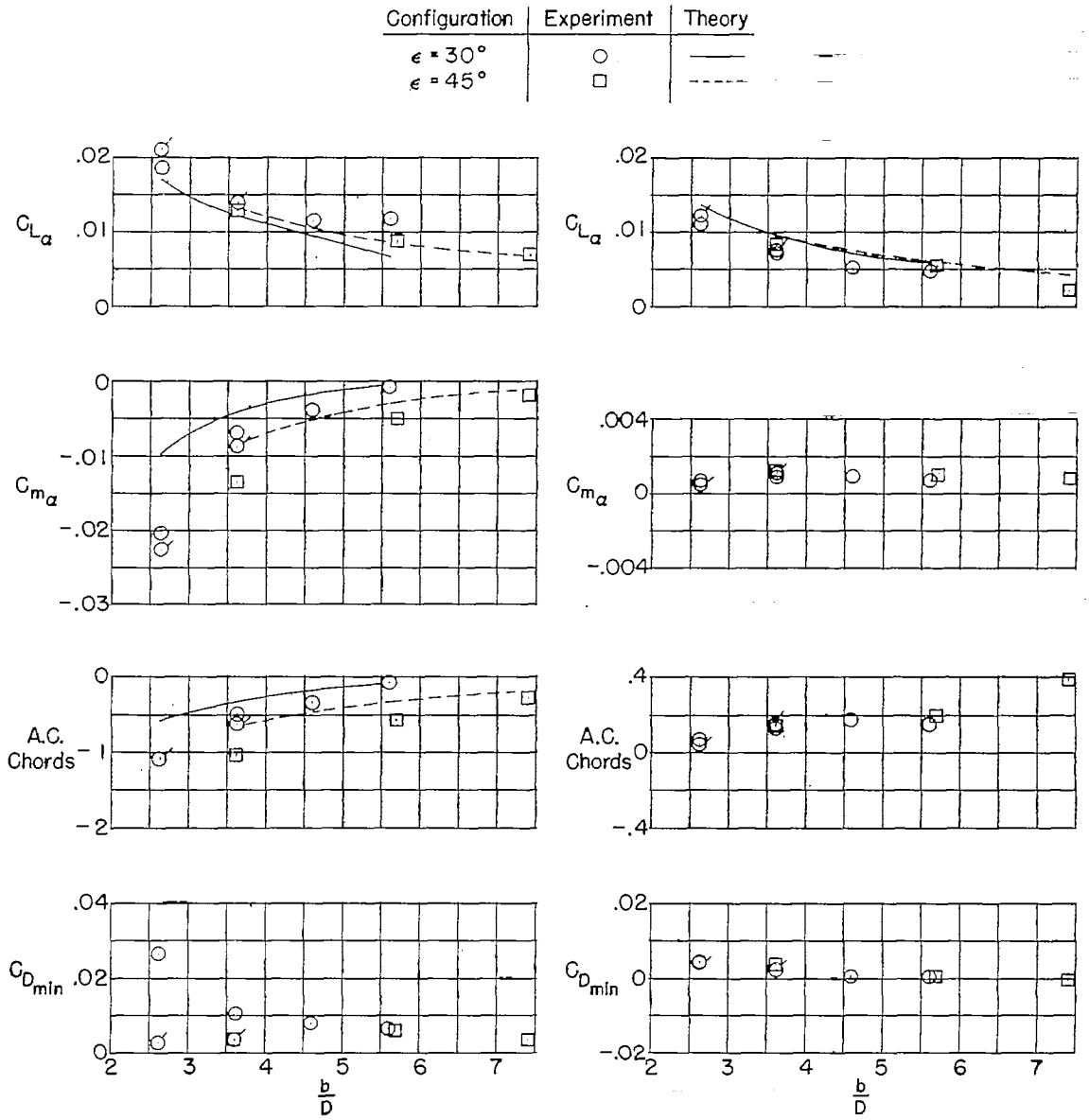

(a) b(w). Based on exposed wing area.

(b) w(b). Based on exposed wing area.

Figure 25.- Interference quantities as a function of b/D for b(w) and w(b) with the n = 10.27 body. Flagged symbols denote n = 9.13 body.

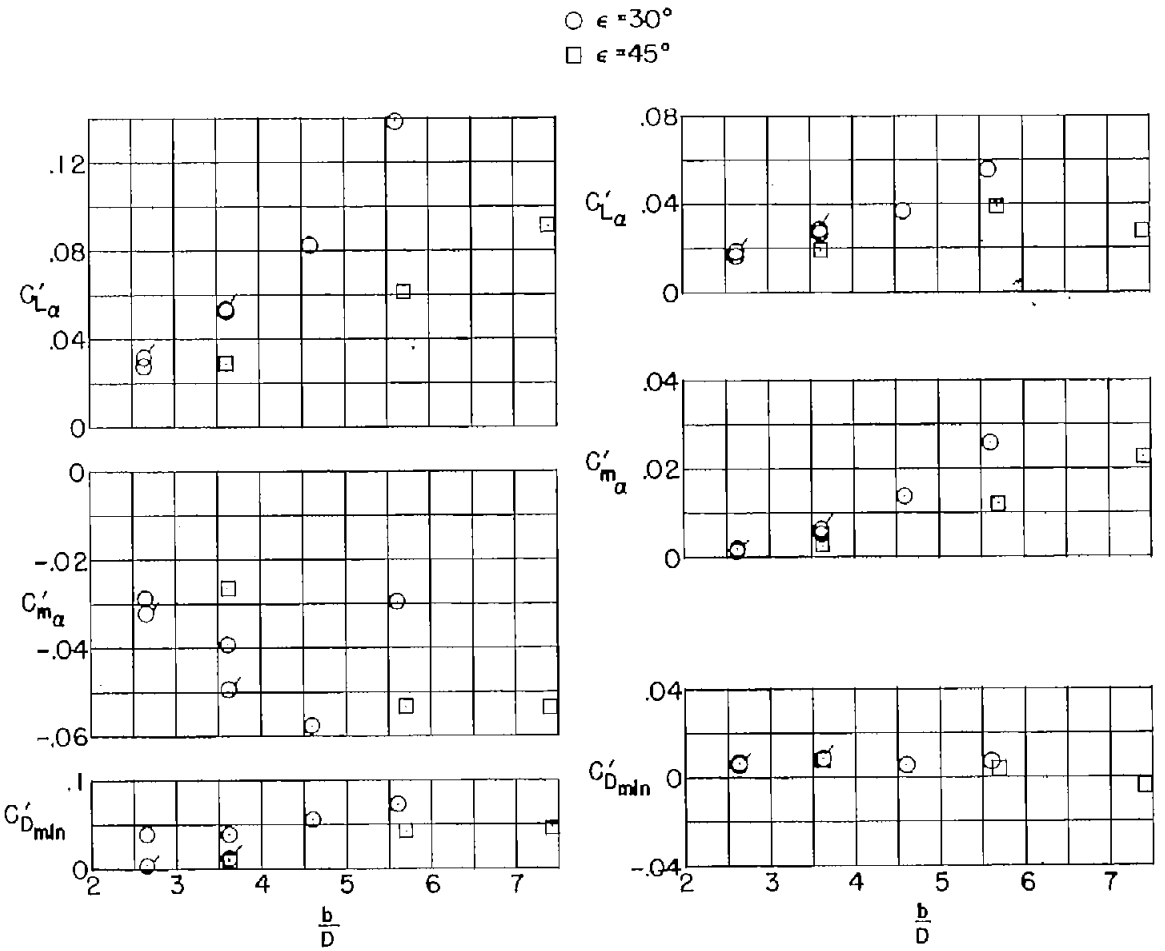

(c) b(w). Based on maximum body frontal area and maximum body diameter.

(d) w(b). Based on maximum body frontal area and maximum body diameter.

Figure 25.- Concluded.

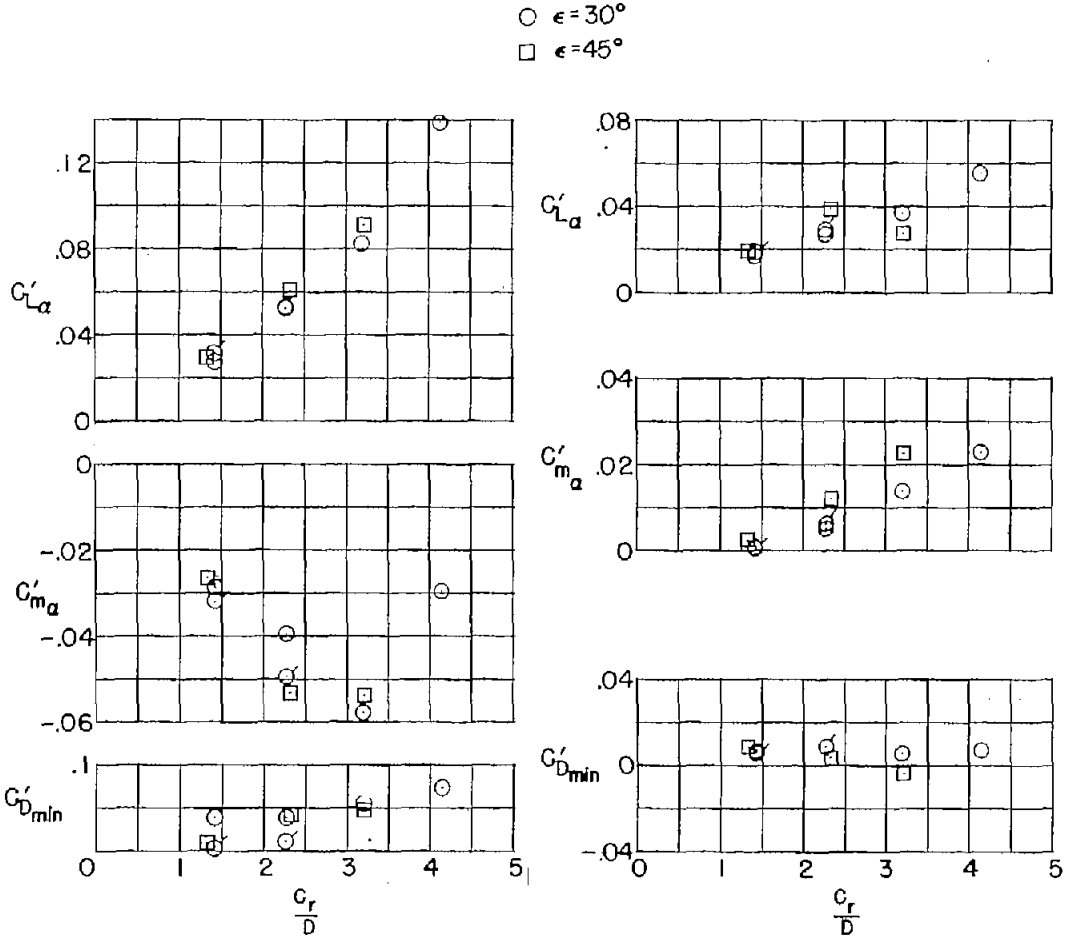

(a) b(w). (b) w(b).

Figure 26.- Interference quantities as a function of c_r/D for b(w) and w(b) with the n = 10.27 body. Flagged symbols denote n = 9.13 body. Based on maximum body frontal area and maximum body diameter.

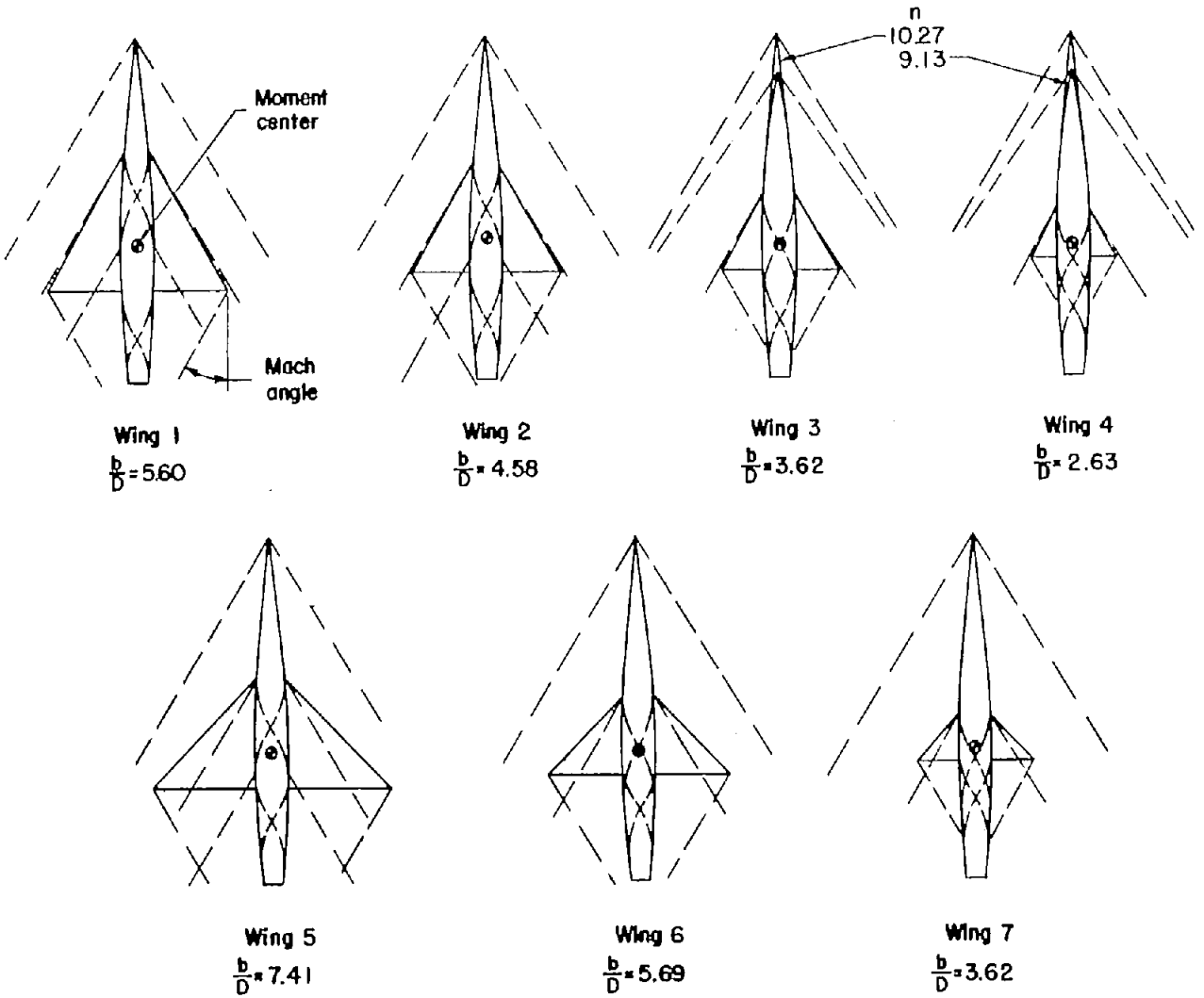

Figure 27.- Approximate location of nose shocks and Mach lines on the series of triangular wing and body combinations at M = 1.94.

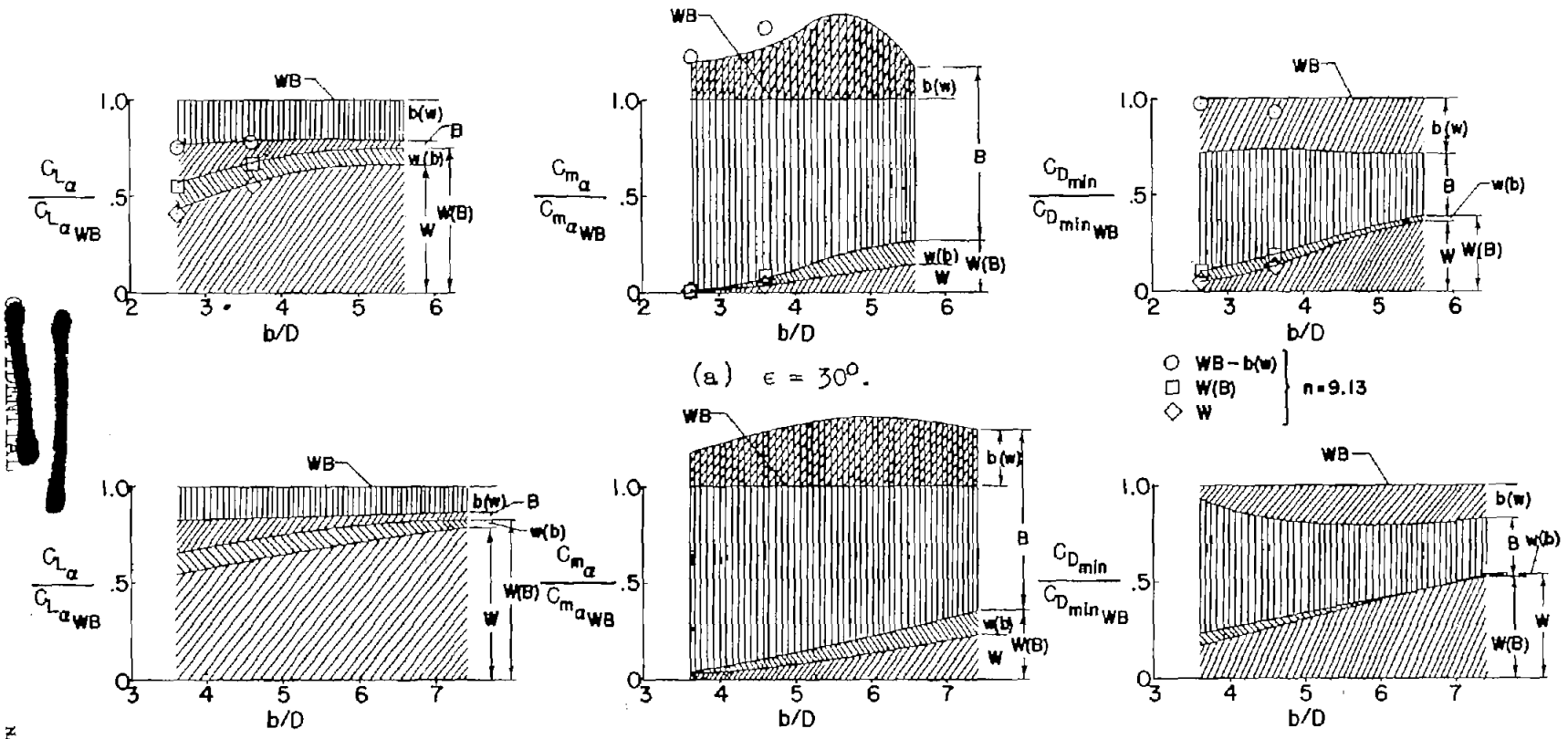

Figure 28.- Incremental and interference quantities with the n = 10.27 body and n = 9.13 body. Symbols denote n = 9.13 body.